EPA-R2-72-019
February 1972

PB 211 504

Reproduced by
NATIONAL TECHNICAL
INFORMATION SERVICE
U S Department of Commerce
Springfield VA 22151

BIBLIOGRAPHIC DATA SHEET	1. Report No. EPA-R2-72-019	2. 128	3. Recipient's Accession No. PB-211 504
4. Title and Subtitle: Electron Paramagnetic Resonance (EPR) Investigation of Limestones and Their Calcines and Correlation with Reactivity with Acid Gases			5. Report Date: 18 February 1972 6.
7. Author(s): Nicholas A. Ashford and Frank H. Jarke			8. Performing Organization Rept. No. IITRI-C6241-7
9. Performing Organization Name and Address: IIT Research Institute, 10 West 35th Street, Chicago, Illinois 60616			10. Project/Task/Work Unit No. 11. Contract/Grant No. 68-02-0208
12. Sponsoring Organization Name and Address: ENVIRONMENTAL PROTECTION AGENCY, 411 West Chapel Hill Street, Durham, North Carolina 27701			13. Type of Report & Period Covered: Final 14.

15. Supplementary Notes

16. Abstracts

A research program was undertaken to investigate a selected set of calcined and uncalcined carbonate rock samples by electron paramagnetic resonance (EPR) spectroscopy in order to (a) assist in the characterization of marls and chalks to identify properties which account for their high reactivity with SO2, (b) establish a semi-quantitative basis for evaluating a crystalline order of limestones to predict their reactivity with acid gases, (c) investigate the effect of altering the calcination temperature on the crystalline structure of calcines in order to identify those properties which account for the varying reactivity and deadburning, and (d) investigate the effects of slaking on the crystalline parameters of calcines produced at different temperatures in order to support wet limestone scrubbing process development using manganese ions as a probe of calcium carbonate crystallinity, the fitting of manganese EPR line width data to the SO_2 reactivity and capacity data resulted in correlation coefficients of r = 0.55 and 4 = 0.49 respectively. No significant EPR linewidth correlation was found for the reactivity and capacity of calcined materials

17. Key Words and Document Analysis. 17a. Descriptors

Air pollution
Electron paramagnetic resonance (EPR)
Spectroscopy
Limestone
Reactivity
Slaking
Calcines
Sulfur dioxide

17b. Identifiers/Open-Ended Terms

17c. COSATI Field/Group 13B, 7D 1a

18. Availability Statement	19. Security Class (This Report)	21. No. of Pages
Unlimited	UNCLASSIFIED	74
	20. Security Class (This Page) UNCLASSIFIED	22. Price

MANAGEMENT SUMMARY

The investigations reported herein were performed in the Physical Chemistry Section of the Chemistry Division of IIT Research Institute. Dr. Nicholas A. Ashford, Research Chemist, acted as project leader and was responsible for the experimental design and interpretation. Mr. Frank H. Jarke, Assistant Chemist, performed the experimental work and assisted in the experimental design and interpretation. Dr. Elliott Raisen, Manager of Physical Chemistry, was responsible for general administration of the program.

FOREWORD

This report No. IITRI-C6241-7 is the Final Technical Report on IITRI Project C6241, Contract No. 68-02-0208, entitled "Electron Paramagnetic Resonance (EPR) Investigation of Limestones and Their Calcines and Correlation with Reactivity with Acid Gases". This program is being conducted by IIT Research Institute, 10 West 35th Street, Chicago, Illinois for the Environmental Protection Agency, Durham, North Carolina 27701, and covers the period from June 23, 1971 through January 22, 1972. The program monitor is Dr. Dennis C. Drehmel.

Respectfully submitted,

IIT RESEARCH INSTITUTE

N A Ashford

Nicholas A. Ashford
Research Chemist
Physical Chemistry Research

Frank H Jarke

Frank H. Jarke
Assistant Chemist
Physical Chemistry Research

Approved by:

Elliott Raisen

Elliott Raisen
Manager
Physical Chemistry Research

NAA:FHJ:rta

ABSTRACT

A research program was undertaken to investigate a selected set of calcined and uncalcined carbonate rock samples by electron paramagnetic resonance (EPR) spectroscopy in order to (a) assist in the characterization of marls and chalks to identify properties which account for their high reactivity with SO_2, (b) establish a semi-quantitative basis for evaluating a crystalline order of limestones to predict their reactivity with acid gases, (c) investigate the effect of altering the calcination temperature on the crystalline structure of calcines in order to identify those properties which account for the varying reactivity and deadburning, and (d) investigate the effects of slaking on the crystalline parameters of calcines produced at different temperatures in order to support wet limestone scrubbing process development.

Using Mn^{++} as a probe of calcium carbonate crystallinity, the fitting of Mn^{++} EPR linewidth data to the SO_2 reactivity and capacity data resulted in correlation coefficients of $r=0.55$ and $r=0.49$ respectively. No significant EPR linewidth correlation was found for the reactivity and capacity of calcined materials. However, in a calcined series in which the calcination temperature was varied producing variations in density, a good correlation of the EPR linewidths was found with the density data. Hydration of calcined materials produces a hydrated site for the Mn^{++} which gives a different and distinguishable EPR spectrum than that for Mn^{++} in unhydrated sites. Quantitative measurement of the degree of hydration was therefore possible.

SUMMARY OF FINDINGS

1. The fitting of Mn^{++} EPR linewidth data to the SO_2 reactivity and capacity data resulted in correlation coefficients of r=0.55 and r=0.49 respectively, for all the carbonate samples except dolomites. From the qualitative observations that within a carbonate type, the sharper and better-resolved Mn^{++} lines occur for the more reactive material, it is believed that better linewidth correlation might be found within any carbonate type. Variations of the inherent structure of even a perfect lattice from carbonate type to carbonate type might account for a not-larger correlation among all the samples.

2. The effect of room temperature ultraviolet-irradiation of Michigan Marl (Type 1, #2129) under high vacuum is significant. Fe^{++} is promoted to Fe^{+++} without (presumably) a change in the surface area or pore volume. The increase in Fe^{+++} is maintainable in air - i.e. stable. This suggests that (permanent) decoration of the defect state of the carbonates may be possible in order to utilize photo-created Fe^{+++} as a measure of crystallinity, as well as Mn^{++}.

3. In the Type 1 Iceland spar calcine, the low SO_2 capacity anisotropic 1700°F calcine with a high degree of strain shows no Fe^{+++} center while the higher-capacity isotropic 1800°F calcine yields the Fe^{+++} center. Thus, while Fe^{+++} seems to

be an indicator of SO_2 capacity, its role is by no means clear at this time. However, there are two other EPR parameters relating to impurity Mn^{++} ions which may indicate the degree of crystallinity of the materials: transitions which are quantum-mechanically forbidden and the fine structure. As expected, the 1800°F calcine with the more perfect lattice results in weaker forbidden transition intensitites and stronger transitions corresponding to the fine structure.

4. In the 2061 calcine series, in which five different temperatures were used to calcine the same carbonate material, the Mn^{++} linewidths did prove to correlate well with the density data. The SO_2 reactivity and capacity data did not correlate with the Mn^{++} linewidths either in this series or in any of the calcines investigated. Reactivity, however, depends on both the density and the initial crystallinity, the latter to which the Mn^{++} EPR is not sensitive.

5. The EPR results on the calcined samples after soaking with water and drying indicate the presence of a second site for Mn^{++} which is most probably the hydrated oxide site. The near linear relationship of the EPR data for the variable temperature Series 2061, 2062 and 2069 with the results of the slaking test is independent evidence of the assignment of the new EPR lines to Mn^{++} in hydrated sites. The small shift observed for the field positions of the

"second phase" is almost conclusive by itself.

6. Increasing the calcination temperature of the three different series 2061, 2062 and 2069 results in an increase in the Fe^{+++}, except for the highest temperature in each series - 3200°F. Since the Fe^{+++} level in calcines seems to be related to the calcination temperature as a general phenomena, it may be possible to utilize EPR to find the optimum calcination temperature. Most of the iron is probably present as Fe^{++}, which is not observed by EPR in these materials.

TABLE OF CONTENTS

		Page
Management Summary		i
Abstract		ii
Summary of Findings		iii
I.	INTRODUCTION	1
II.	EXPERIMENTAL PROCEDURE	6
A.	Samples	6
B.	EPR Procedure	6
C.	Ultraviolet-Visible Irradiation of Sample Type 11	6
D.	Slaking Test	10
III.	EXPERIMENTAL RESULTS	11
A.	Carbonate Samples	11
B.	Calcined Samples	15
IV.	DISCUSSION OF RESULTS	25
A.	Carbonate Samples	25
B.	Calcined Samples	26
C.	Slaking Test	27
D.	The Role of Fe^{+++} in the Calcines	27
V.	RECOMMENDATIONS AND CONCLUSIONS	28
References		30
APPENDIX A		
APPENDIX B		
APPENDIX C		

LIST OF TABLES AND FIGURES

Table		Page
I	Carbonate Samples	7
II	Calcined Samples	8
III	Calcined Samples, Variable Temperature Series	9
IV	Regression Coefficients for EPR Linewidths L to the Reaction Data	12
Figure		
1	SO_2 Reactivity in Differential Test Versus EPR Linewidth Parameter of Selected Limestones. Correlation Coefficient is 0.55.	13
2	Sorption Capacity, Fixed Bed, Versus EPR Linewidth Parameter of Selected Limestones. Correlation Coefficient is 0.49	14
3	SO_2 Reactivity in Differential Test Versus EPR Linewidth Parameter of Selected Calcines	17
4	Sorption Capacity, Fixed Bed, Versus EPR Linewidth Parameter of Selected Calcines	18
5	Density Versus EPR Linewidth for Series 2061 Calcines	19
6	Effect of Calcination Temperature on Fe^{+++} Center in Calcines	20
7	Relationship of Mn^{++} EPR Signal Intensities to the Slaking Test Data	24

ELECTRON PARAMAGNETIC RESONANCE (EPR) INVESTIGATION OF LIMESTONES AND THEIR CALCINES AND CORRELATION WITH REACTIVITY WITH ACID GASES

I. INTRODUCTION - PURPOSE AND SCOPE OF WORK

Abatement of atmospheric pollution by sulfur dioxide or hydrogen sulfide has received particular attention with emphasis based on reactions of the pollutants with limestone. The limestone wet scrubbing process, limestone fluidized bed combustors and coal gasification are currently under intensive investigation and development. Limestones, dolomites and their derivatives as naturally occurring substances show a wide range of reaction rates as well as capacity for acid gas sorption.

Mechanistic and kinetic studies were initiated on the dry injection process. Borgwardt (Ref. 1,2) has shown that limestone absorbs SO_2 by a mechanism involving at least two consecutive steps; (1) dissociation of the calcium carbonate,(2) followed by reaction of CaO with sulfur dioxide. He suggested (Ref. 1) that some reaction takes place within the interior structure of the solid and that the relative importance of the internal reaction becomes greater as the particle size decreases. He subsequently demonstrated (Ref. 2), that the rate of sorption is limited by a first-order reaction which occurs throughout the internal pore structure of small particles. There is a strong influence of physical properties

upon the sorption of SO_2. Small pores and large surface areas lead to high reaction rates while large pores lead to high capacity. Stones of varying geological type yield calcines of distinctly different physical properties which show correspondingly large differences in both rate of reaction and total capacity for SO_2 sorption (Ref. 2). Ishida,et al (Ref. 3) have shown that there is an unreacted core, the size of which may depend on the particle size (and porosity) of the particle itself.

Murthi,et al (Ref. 4) have recently reported studies on the SO_2 sorption capacity of limestones and dolomites as a function of calcination time and temperature in the dry injection process. The role of surface area, porosity, and chemical composition on the sorbent capacity was discussed. The effect of moisture and of the presence of iron oxide in the samples was also reported.

Harvey (Ref. 5, 6) has carried out extensive studies of the petrographic and mineralogical characteristics of carbonate rocks related to sorption of sulfur oxides in flue gases. Detailed petrographic, mineralogical, and chemical analyses of 26 carbonate rocks were made and compared with the capacity (3-1/2 hr. reaction period) and differential reactivity (120 sec. reaction period) of calcined specimens for sorption of sulfur dioxide (SO_2). Three petrographic and chemical properties appear to be useful indexes of the SO_2 sorption

capacity: the pore volume, the grain size, and the sodium oxide content of the rocks. The larger the pore volume, the greater was the sorption capacity of the rock. In general, the finer the grain size of the rock, the higher was the sorption capacity. Of the chemical elements analyzed, only sodium showed a correlation trend with the SO_2 test data. The sodium present in the samples increased with increasing sorption capacity. Unlike the sorption capacity tests, the differential reactivity tests showed little or no correlation with petrographic and chemical properties.

Relatively high SO_2 reactivity was observed for chalks, calcareous marls, and oolitic aragonite sand samples and is believed due mainly to the high pore volume and fine grain size of these carbonate rocks.

Drehmel (Ref. 7) reported studies of the chemical and physical properties of three series of calcined carbonates (two limestones and one dolomite) as they pertain to "dead-burning" in the dry injection process. A high degree of intercorrelation was found between sulfur dioxide reactivities, surface area and pore volume.

Drehmel (Ref. 8) has recently compared carbonate rock types as to their sulfur dioxide removal efficiencies in a batch scrubber and found the best types to be marl and chalk and the worst marble and magnesite. For calcined limestone, the change in scrubbing efficiency with calcination temperature was found to be due to the resulting

change in surface area or pore volume. At higher temperatures where surface area was lost, reactivity was lost. The variation in scrubbing efficiency with different calcined limestone types was found to be a function of both the surface area and pore volume.

Much of the primary reactivity and capacity data referred to in this report is also to be found in a recent technical report issued by EPA (Ref. 9).

The purposes of the present investigation of a selected set of limestone and calcine samples by electron paramagnetic resonance (EPR) spectroscopy were to (a) assist in the characterization of marls and chalks to identify properties which account for their high reactivity, (b) establish a semi-quantitative basis for evaluating a crystalline order of limestones to predict their reactivity with acid gases, (c) investigate the effect of altering the calcination temperature on the crystalline structure of calcines in order to identify these properties which account for the varying reactivity and deadburning, and (d) investigate the effects of slaking on the crystalline parameters of calcines produced at different temperatures in order to support wet limestone scrubbing process development.

The theory of electron paramagnetic resonance (EPR) spectroscopy and its application to the characterization of solid-state materials are provided in Appendix A.

Pure $CaCO_3$ exhibits no EPR absorption, unless the material is irradiated. However, both Mn^{++} and Fe^{+++} occur naturally in limestones as substitutional ions for Ca^{++} and thus act as paramagnetic probes of the crystal structure. It is these probes which provide the basis of the present investigation.

It is interesting to note that scientists in India (Ref. 10) have suggested using the Mn^{++} concentration determined by EPR techniques in calcium carbonate materials as an aid to manganese ore prospecting and also as an index for establishing the relative ages of samples belonging to unclassified geological periods.

II. EXPERIMENTAL PROCEDURE

A. Samples

The polycrystalline carbonates and calcines which were examined are listed in Tables I, II and III.

B. EPR Procedure

The polycrystalline samples were placed in Varian 9.5 GHz quartz sample tubes, ≈ 3 mm ID and the tubes evacuated to a pressure less than 50 microns. The EPR spectra were obtained at liquid nitrogen temperatures using a standard cold finger dewar placed in the Varian Model V-4531 multipurpose cavity operated at a microwave frequency of ≈ 9140 MHz. Superheterodyne detection and 400 Hz field modulation were employed. The spectra were recorded on a Varian X-Y recorder using the magnetic field as a base. See Appendix A for a more detailed discussion of EPR spectroscopy and its application to solid-state materials.

C. Ultraviolet-Visible Irradiation of Sample Type 11

Ultraviolet-visible irradiation of the sample Type 11 in a suprasil EPR tube under high vacuum (10^{-7} torr) was performed utilizing unfiltered light from an Osram 500 watt point-source lamp collimated with a four-inch diameter fused silica lens (focal-length four inches). The lens was placed at approximately twice the focal length from the lamp providing a one-to-one magnification of the point-source arc whose image was entirely contained within the polycrystalline sample area. The irradiation was carried out for 63 hrs at ambient temperatures outside the dewar and cavity. EPR measurements at liquid nitrogen temperatures were carried out immediately after the irradiation and again, one week later.

TABLE I

CARBONATE SAMPLES*

IGS Type**	EPA Nomenclature	Size	Description
Type 1	#2201	150/170	Iceland spar, calcite
Type 3	#2203	150/170	Limestone, coarse grained high purity
Type 4	#2204	150/170	Limestone, fine grained high purity
Type 5	#2205	150/170	Dolomite, reef type high purity
Type 6	#2206	150/170	Dolomite
Type 7	#2207	Hand Ground	Magnesite, fine grained high purity
Type 8	#2208	150/170	Aragonite
Type 10	#1336	150/170	White crushed marble
Type 11***	#2129	150/170	Michigan marl
	#2077	150/170	Austin chalk
Type 12	#2081	150/170	Kansas chalk
	#2109	150/170	New York marl
	#2080	150/170	Northeastern Ohio marl

* Supplied by EPA and Described by Harvey[6]

** Illinois Geological Survey nomenclature[6]

*** Ultraviolet decoration performed

TABLE II

CALCINED SAMPLES*

IGS Type	EPA Nomenclature	Size	Calcination Temperature	Description of the Precuisor Carbonate
Type 1	#2201	150/170	1700°F	Iceland spar, calcite
		10/28	1800°F**	
Type 3	#2203	150/170	1700°F	Limestone, coarse grained, high purity
Type 4	#2204	150/170	1700°F	Limestone, fine grained, high purity
Type 5	#2205	150/170	1700°F	Dolomite, reef type, high purity
Type 6	#2206	150/170	1700°F	Dolomite
Type 9	#2209		1700°F	Dolomite
Type 10	#1336	150/170	1700°F	White crushed marble
Type 11	#2129	42/65	1700°F	Michigan marl
	#2077	***	***	Austin chalk
Type 12	#2081	***	***	Kansas chalk
	#2109	***	***	New York marl
	#2080	***	***	Northeastern marl

* All samples prepared by EPA (2 hours at temperature)

** Contaminated with light-green colored material

*** Data unknown

TABLE III

CALCINED SAMPLES*, VARIABLE TEMPERATURE SERIES

EPA Nomenclature	Size	Temperature, °F	Description
#2061	170/200	1700** 2000** 2300** 2600** 3200**	Fredonia White Limestone
#2062	-170	1700** 2000** 2300 2600 3200**	Cedar Bluff Limestone
#2069	-170	1700** 2000** 2300 3200**	James River Dolomite

* Supplied by EPA

** Slaking Test Performed

The sample was then exposed to air at atmospheric pressure for one hour and then repumped to 10^{-7} torr in order to investigate the air-stability of the irradiation created Fe^{+++}.

D. Slaking Test

Selected calcined samples listed in Table III were placed on pyrex watch glasses and were investigated according to the slaking test conceived by T. D. Womble of T.V.A. and used by EPA. Since the samples had not been received from EPA sealed from the air, they were preheated at 650°C for three hours to dispel any absorption of atmospheric water. After cooling to room temperature in a dessicator over P_2O_5, water was added to the samples in the ratio 1 ml/g sample or 5 ml/g sample and the samples then soaked for times of 30, 60, or 120 minutes. The wet samples were then dried in an oven at 240°C for two hours, after which they were removed and again placed over P_2O_5 in a dessicator where they cooled. They were then reexamined for EPR absorption at liquid nitrogen temperatures.

III. EXPERIMENTAL RESULTS

A. Carbonate Samples

1. EPR Spectra

The six main transitions characteristic (Ref. 11) of Mn^{++} are observed in all the carbonates except Type 7(magnesite). A well-resolved spectrum in Type 10 (marble) is shown in Figure B1 of Appendix B*. Sample Type 11 (Michigan marl) exhibts more poorly resolved Mn^{++} transitions as is shown in Figure B2, but also displays a center at g = 2.0029 which we attribute to Fe^{+++}(Ref. 12). The limestones, chalks and marls all exhibit similar, but not identical, spectra with the g-value for Mn^{++} = 2.0048. Representative spectra are shown in Appendix B. Aragonite and the dolomites exhibit slightly different spectra, which are also shown in Appendix B. The role of Fe^{+++} in the carbonates was not fully investigated, but it was observed in samples Type 1, 8 and 11.

2. EPR Linewidth Analysis and Correlation With Chemical Reaction Data

The highfield "line" of the six Mn^{++} transitions was chosen for linewidth analysis since it was the best resolved. The theory and discussion of linewidth analysis is given in Appendix A.

---

* In the remainder of the text, Figures in Appendix B will be designated Bn while Figures in the main text will be designated by an integer n, as is the usual practice.

A least-squares linear regression analysis was done on eight of the samples listed (Table I). The two dolomites were not included in the fitting as their variance from the set seemed to be significant and because the linewidths may be affected by the presence of Mg^{++} in the dolomite structure.

Three different EPR parameters were chosen and each fitted to the reactivity and capacity data of Table 14 of Reference 6. The three parameters are designated L_1, L_2 and L_3 and are discussed in Appendix A. The correlation coefficients for the fitting of the linewidths to the reactivity and capacity data are listed in Table IV. The data for L_1 are presented in Figures 1 and 2. The dolomite data -"D"-have been circled to indicate that they were not used in the fitting.

TABLE IV

REGRESSION COEFFICIENTS FOR EPR LINEWIDTHS L TO THE REACTION DATA

Reaction data	L_1	L_2	L_3
reactivity	0.55	0.20	0.18
capacity	0.49	0.45	0.17

3. Ultraviolet-Visible Irradiation of Sample Type 11

The EPR spectra of the material before and after

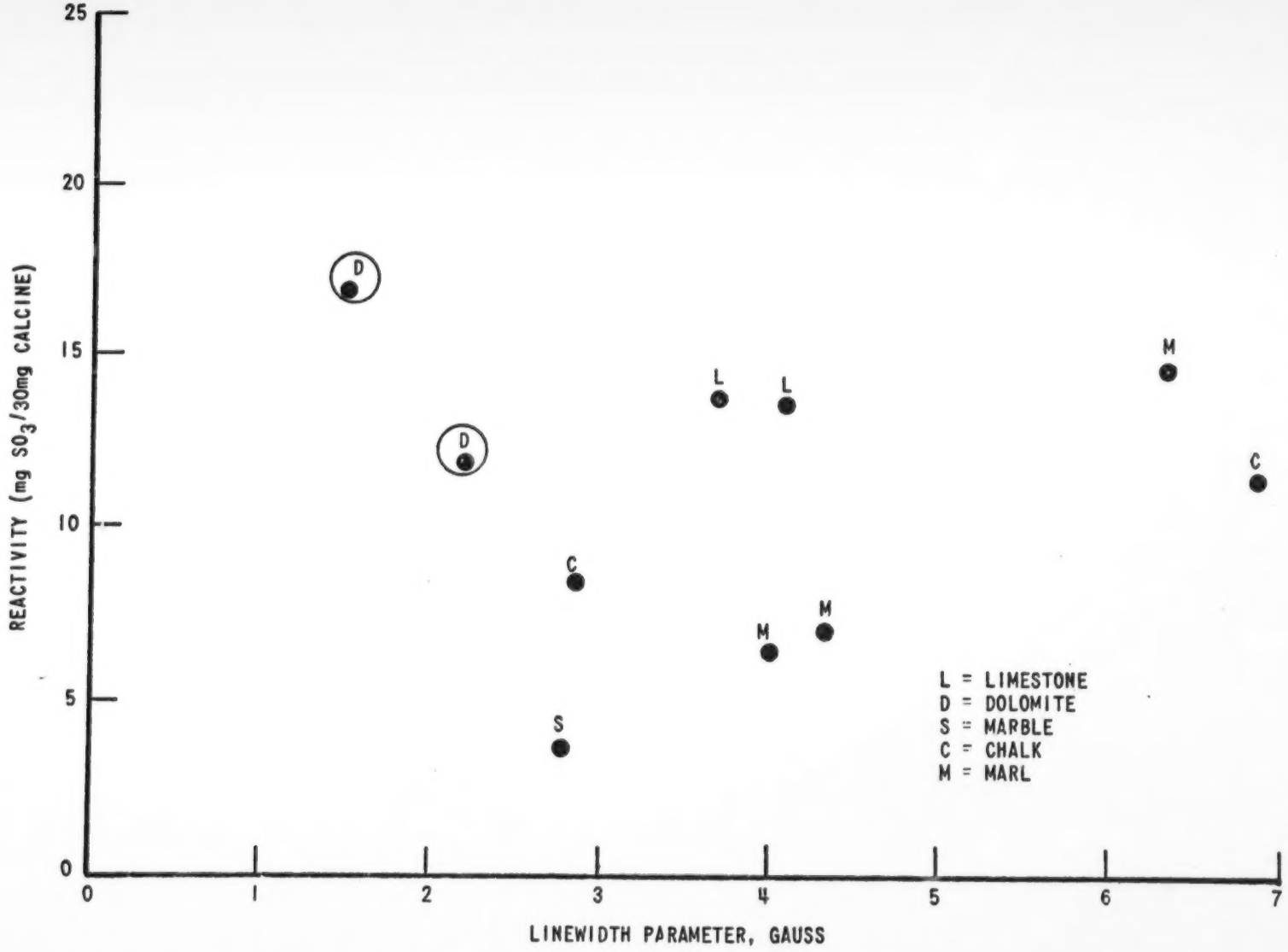

Figure 1 SO_2 REACTIVITY IN DIFFERENTIAL TESTS VERSUS EPR LINEWIDTH PARAMETER OF SELECTED LIMESTONES. CORRELATION COEFFICIENT IS 0.55.

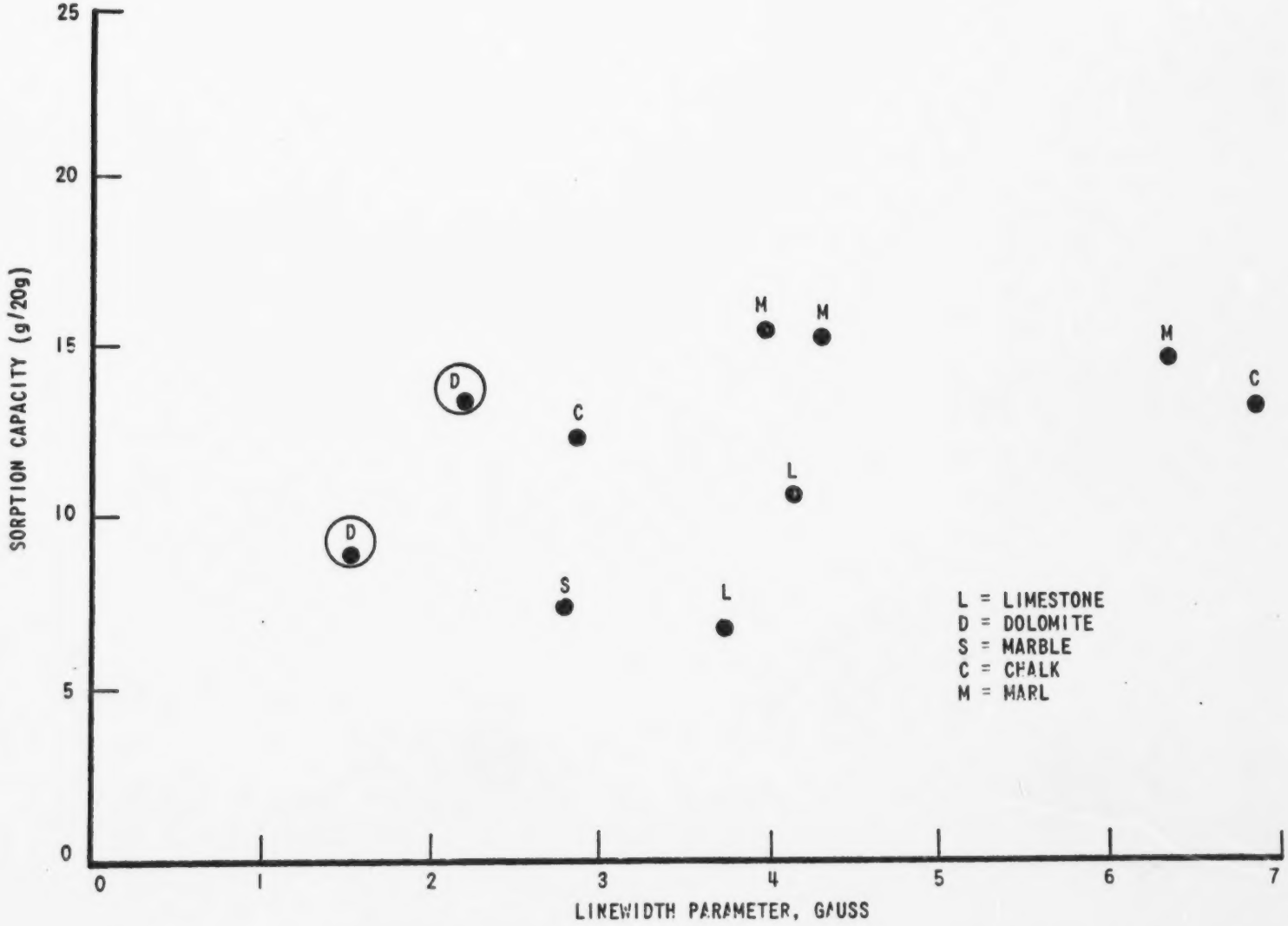

Figure 2 SORPTION CAPACITY, FIXED BED, VERSUS EPR LINEWIDTH PARAMETER OF SELECTED LIMESTONES. CORRELATION COEFFICIENT IS 0.49.

63 hrs. irradiation at ambient temperatures are shown in Figures B3 & B4, respectively. The Fe^{+++} is increased by the irradiation and remained stable for more than a week under high vacuum ($< 10^{-7}$ torr). Furthermore, the subsequent admission of air at atmospheric pressure to the sample for one hour did not result in any reduction in signal intensity.

B. Calcined Samples

1. EPR Spectra

Six Mn^{++} transitions were observed in the calcines with slightly different g-values (2.0069 for the calcites) and splittings than are found in the carbonates. A typical spectrum in the 1700°F calcine of Type 1 (Iceland Spar Calcite) is shown in Figure B5. When Type 1 calcined at 1800°F, a center at g = 2.0047, characteristic of Fe^{+++} (Ref. 13) is also observed. (The sample also exhibits another strong line, believed to be an impurity). Aside from the appearance of the Fe^{+++} in the 1800°F calcine along two other significant differences exist between the two calcines. First, closer examination of the two minor peaks flanking the place where Fe^{+++} is observed shows that the peaks are stronger in the 1700°F calcine (Figures B7 & B8). Secondly, the structure underlying each of the six main Mn^{++} peaks is stronger and better resolved in the 1800°F cal-

cine. The fifth-highest main Mn^{++} line is shown in (Figures B9 & B10) Type 1 was the only material for which a 1700°F and 1800°F calcine was available for investigation. However, the other 1700°F calcines showed the main Mn^{++} transitions and Fe^{+++} was also observed in Type 3, 5, 6, 10 and 11.

2. EPR Linewidth Analysis

The linewidth of the low field Mn^{++} transition were measured for all the samples in Table II and in Figures 3 and 4 are plotted against the reactivity and capacity data of Table 14 of Reference 6. No regression analysis was attempted since the scatter is large, but the chalks did appear to have rather large linewidths, indicative of their 'unconsolidated' nature.

3. Variable Temperature Series

The Series 2061 was examined for Mn^{++} linewidth analysis for the five different temperatures (See Table III). While no correlation was apparent between the linewidths and the reactivity or capacity data, a significant relationship was found between the linewidth and the density data found in Table B2-2A of Reference 9. The data is plotted in Figure 5. The spectra of the 2061 series are shown in Figures B11-15.

One striking feature of the series is the variation of the Fe^{+++} intensity as a function of temperature. The signal heights of the Fe^{+++} center normalized to those of the Mn^{++} peak immediately downfield are plotted versus calcination temperature in Figure 6. A qualitative feature of Series 2062

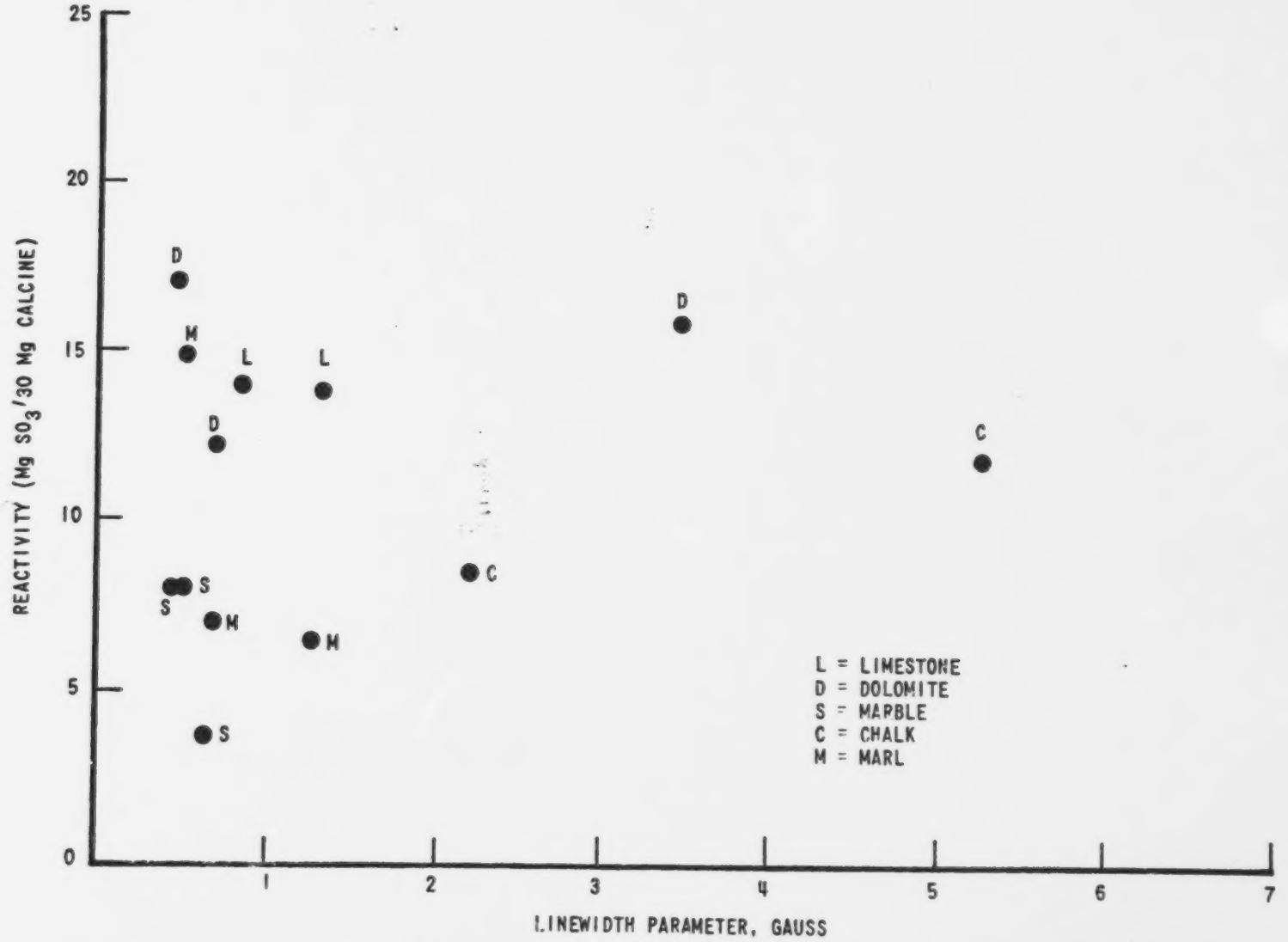

Figure 3 SO_2 REACTIVITY IN DIFFERENTIAL TEST VERSUS EPR LINEWIDTH PARAMETER OF SELECTED CALCINES.

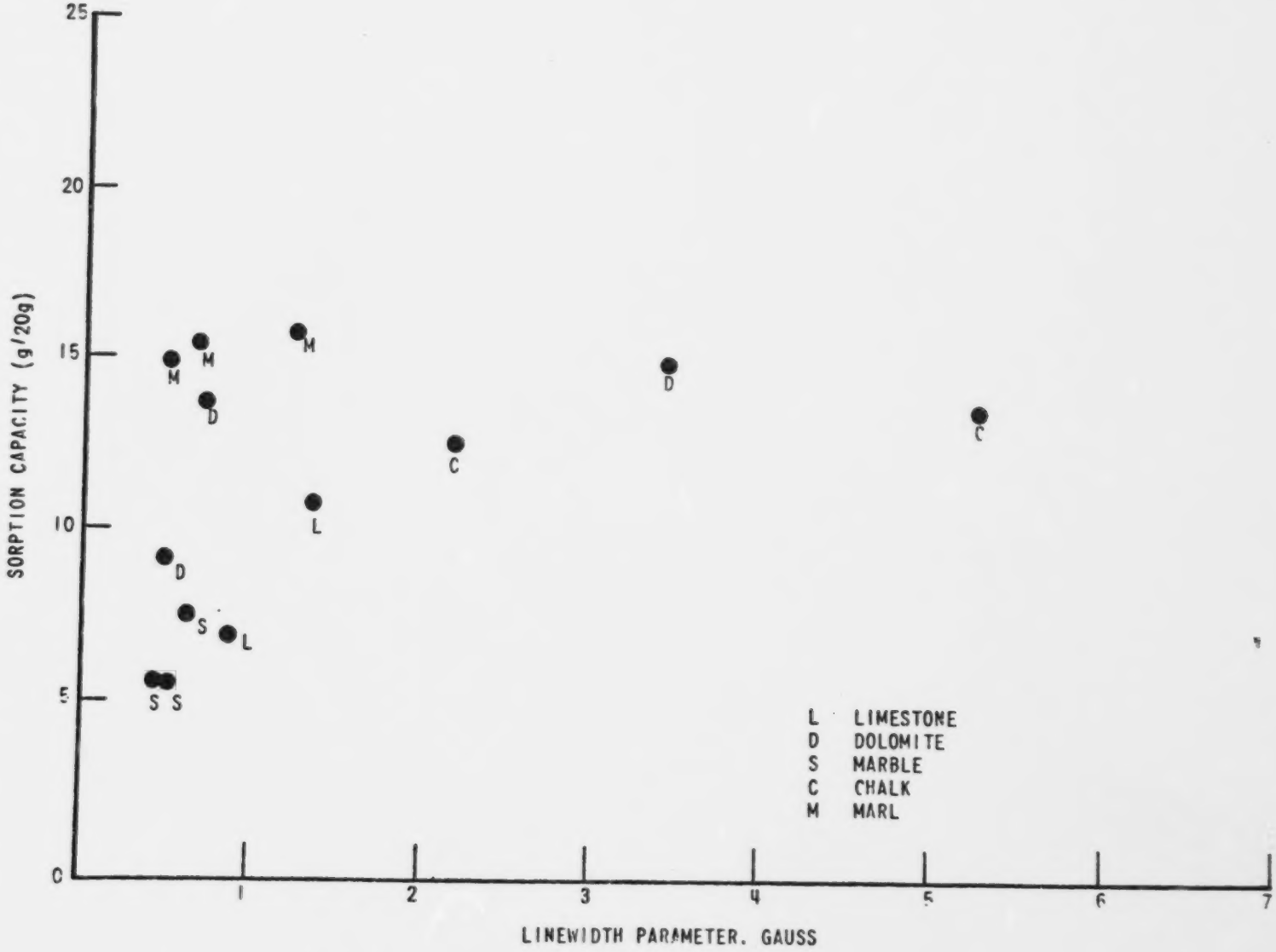

Figure 4 SORPTION CAPACITY, FIXED BED, VERSUS EPR LINEWIDTH PARAMETER OF SELECTED LIMESTONES.

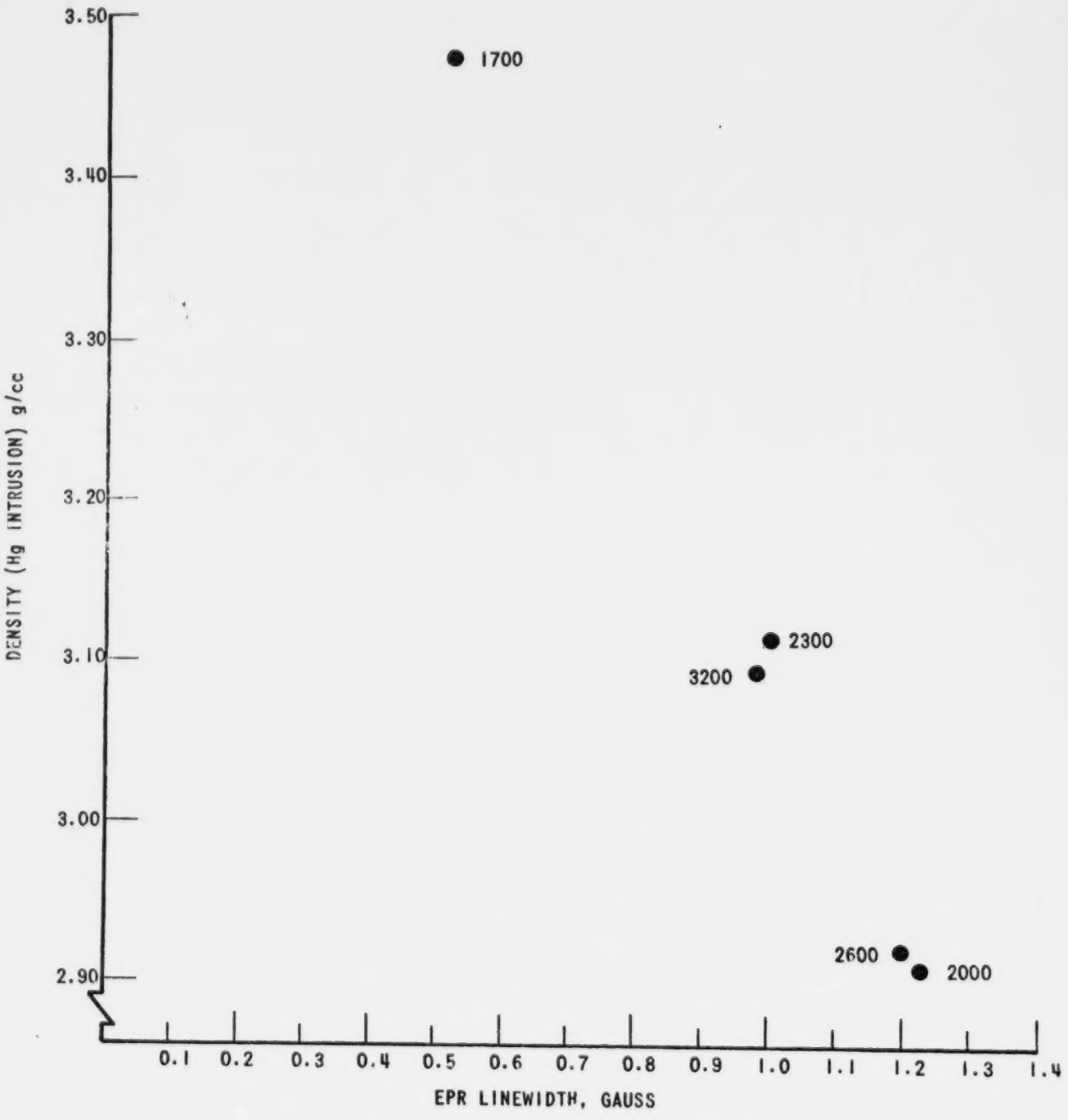

Figure 5 DENSITY VERSUS EPR LINEWIDTH FOR SERIES 2061 CALCINES.

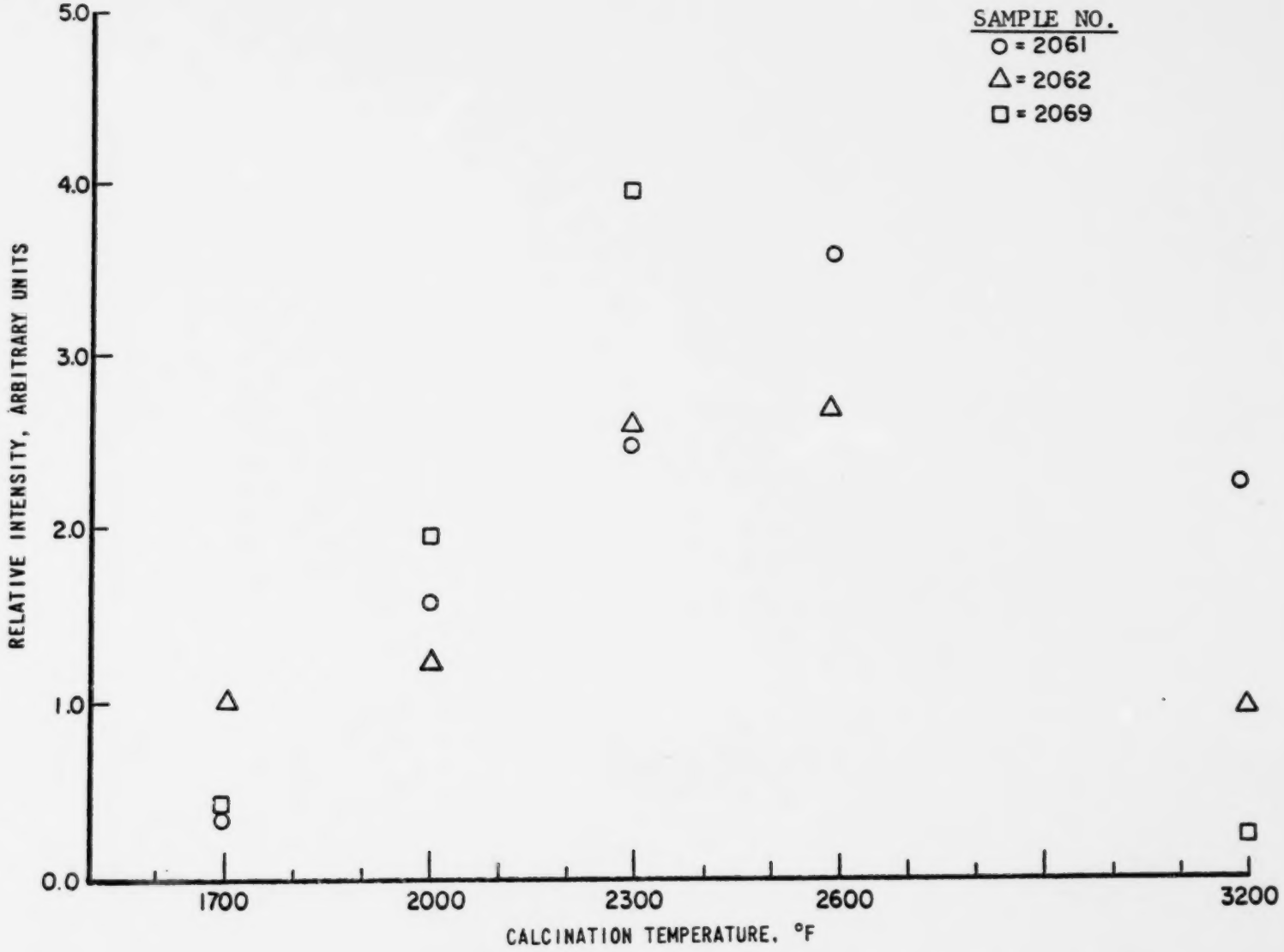

Figure 6 EFFECT OF CALCINATION TEMPERATURE ON Fe^{+++} CENTER IN CALCINES.

and 2069 are similar with the hard-burned sample (3200°F) deviating significantly from a linear relationship.

The spectra of the Fe^{+++} centers in the 2061 and 2062 calcines are similar but differ from what is observed in the 2069 series. There appears to be (at least) one other center overlapping the center identified as Fe^{+++} substituted in the Ca^{++} lattice position.

4. Slaking Test

The samples showed a weight loss on preheating at 650°C and a weight gain after soaking and drying. Different soaking times and volumes were used for the series 2061, 2062 and 2069 and the changes in weights are shown in Tables C-I, C-II and C-III of Appendix C. The results agree generally with those of Drehmel (Ref. 7). The EPR spectra of the dry 1700°F, 2000°F, 2600°F and 3200°F calcines in Series 2061 which had been soaked with 1 ml of water for 60 minutes are shown in Figures B16-19. The spectra showed a "doubling" of the six Mn^{++} lines, indicating that a second site exists for Mn^{++} with hyperfine splittings larger by about 1.5% and a down-field shift in g-value. The behavior of the 2061 series was similar for other soaking times and volumes. The other series, 2062 and 2069 behaved in a similar manner. The spectra for a 5 ml, 120 min. soak for the 1700°F 2061 calcine is shown in Figure B20. The g-value for Mn^{++}, which entirely

is the second site, is equal to 2.0077.

If, the second site is that associated with hydrated CaO, then*

$$\frac{\text{hydrated site signal intensity}}{\text{non-hydrated site signal intensity}} = k \quad \frac{\text{actual \% Wt. gain}}{\text{theoretical \% - actual \% Wt. gain}}$$

*proof:

Concentration of a center $\propto$ Signal Height

$$c = aI$$

$$c' = a'I'$$

where c = concentration of non-hydrated CaO

c' = concentration of hydrated CaO

$$\frac{c'}{c'+c} = \frac{\text{\% wt. gain}}{\text{theoretical maximum \%}}$$

inverting

$$1 + \frac{c}{c'} = \frac{\text{theoretical maximum \%}}{\text{\% wt. gain}}$$

$$\frac{c}{c'} = \frac{\text{theoretical maximum \% - \% wt. gain}}{\text{\% wt. gain}}$$

inverting,

$$\frac{c'}{c} = \frac{\text{\% wt. gain}}{\text{theoretical maximum \% - \% wt. gain}}$$

$$\frac{I'}{I} = \frac{a}{a'} \frac{c'}{c} = k \frac{c'}{c}$$

$$\frac{I'}{I} = k \frac{\text{\% wt. gain}}{\text{theoretical maximum \% - \% wt. gain}}$$

so that the plots of data taken from the spectra (signal intensity) and the Tables C-I, C-II and C-III (slaking test)

should provide independent evidence of whether or not the second site is in fact hydrated CaO. The log-log plot of the data for all experiments is provided in Figure 7, and the slope is seen to be nearly equal to one. Due to overlap of the Mn^{++} transitions in the two sites, the observed deviations are to be expected.

A cursory examination reveals that there does not appear to be any large change in the Fe^{+++} for the 2061 and 2062 series after slaking and drying. However, the 2069 centers increased greatly.

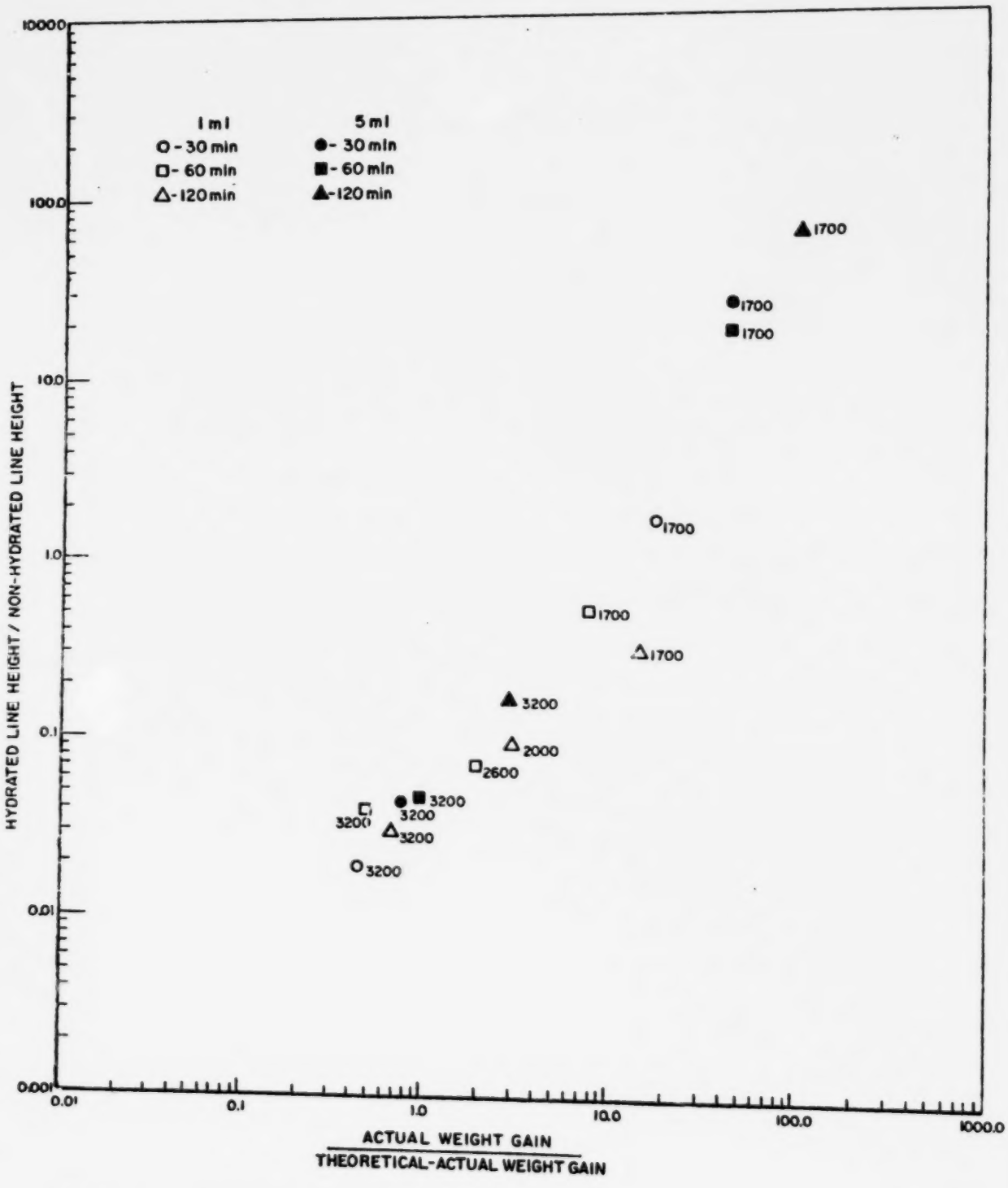

Figure 7 RELATIONSHIP OF Mn^{++} EPR SIGNAL INTENSITIES TO THE SLAKING TEST DATA.

IV. DISCUSSION OF RESULTS

A. Carbonate Samples

The fitting of EPR linewidth data to the reactivity and capacity data resulted in correlations which in the best case ($r = 0.55$ and 0.49) were significant, though not as high as we might have liked. It is interesting though, that both the reactivity and capacity correlations were comparable. The other two parameters chosed for regression analysis, while poorer in result, might have been expected from the less accurate determination of the linewidths in the case of L_2 and L_3, and from the possibility for overlap effects for L_3 as well. From the qualitative observations that within a carbonate type, the sharper and better-resolved Mn^{++} lines occur for the more reactive material, it is believed that better linewidth correlation might be found within any carbonate type. Variations of the inherent structure of even a perfect lattice from carbonate type to carbonate type might account for a not-larger correlation among all the samples.

The effect of ultraviolet-irradiation on Michigan Marl (Type 11, #2129) under high vacuum is remarkable. Fe^{+++} is increased in intensity without (presumably) a change in the surface area or pore volume. The increase in Fe^{+++} is maintainable in air - i.e. stable. This implies that the decoration of the defect structure of carbonates may be investigated by the creation of Fe^{+++} by the photo-oxidation of Fe^{++} and could prove to be as valuable a probe of crystallinity as the Mn^{++}.

B. Calcined Samples

The two Type 1 Iceland Spar Calcines (1700°F and 1800°F) exhibit considerably different external morphology and capacity (Ref. 6). In the Type 1 Iceland spar material, the low capacity anisotropic 1700°F calcine with a high degree of strain shows no Fe^{+++} center while the higher-capacity isotropic 1800°F calcine yields the Fe^{+++} center. Thus while Fe^{+++} seems to be an indicator of capacity, its role is by no means clear at this time. However, there are two other EPR parameters which do indicate the degree of crystallinity of the materials.

The two minor peaks flanking the Fe^{+++} center are essentially quantum-mechanically forbidden transitions whose presence is enhanced by a departure from a cubic environment. Thus, as expected the minor peaks are more intense in the 1700°F calcine.

Furthermore, the structure under the six main Mn^{++} lines is what is known as "fine structure" in spectroscopic language and the better resolution and increase in intensity in the 1800°F calcine is what is expected for a more perfect lattice. It would have been valuable if more of such "pairs" of radically different materials were available for study.

In the 2061 calcine series, the Mn^{++} linewidths did prove to correlate well with the density data. The reactivity and capacity data did not correlate with either the Mn^{++}

linewidths in the calcines of the various types of limestones, or with the density data (Ref. 9). Perhaps, these observations merely reflect that fact that reactivity depends on both the density and the initial crystallinity, the latter to which EPR is not sensitive.

C. Slaking Test

The EPR results on the calcined samples after soaking and drying indicate the presence of a second site for Mn^{++} which is most probably the hydrated oxide site. The relationship of the EPR linewidth data to the slaking test data in Figure 7 is independent evidence of the assignment of the new EPR lines to Mn^{++} in hydrated sites. The small shift observed for the field positions of the "second phase" is almost conclusive by itself.

D. The Role of Fe^{+++} in the Calcines

Since the Fe^{+++} level in the three (unsoaked) series seems to be related to the calcination temperature (Figure 6), it may be possible to utilize EPR to find the optimum calcination temperature. Most of the iron is probably present as Fe^{++}, which is not observed by EPR in these materials.

The appearance of another signal in the 2069 series may be due to Fe^{+++} substituted in Mg^{++} sites. This may not have any bearing on the reactivity of the calcine, however. What is interesting in this series is the great increase in the Fe^{+++} after soaking and drying. It is difficult to satisfactorily rationalize this observation.

V. RECOMMENDATIONS AND CONCLUSIONS

The findings of the investigative effort are well summarized at the beginning of this report and will not be repeated here. However, it is clear that some questions remained unanswered and further research may be expected to be fruitful.

The correlation of EPR linewidths in all the carbonate materials with reactivity and capacity ($r = 0.55$ and $r = 0.49$ respectively), does indicate that higher correlation may be found within a carbonate type. Thus further investigations of a large number of samples for each carbonate type may prove to be of value.

The data show that in the 2061 temperature calcine series, the Mn^{++} linewidths did correlate extremely well with the density data, though not with reactivity or capacity. An attempt to correlate the density data for calcines of all stone types ought to be done. Although the Mn^{++} EPR data seem to be sensitive to the density determinant of reactivity, and not to the initial crystallinity, photocreated Fe^{+++} might prove to be a surface defect and hence sensitive to initial crystallinity. The role of iron in the limestones and their calcines was barely emphasized compared to the Mn^{++} probe, and we believe that Fe^{+++} may turn out to be valuable in ways that Mn^{++} is not as a probe. This is indicated by the comparison of the 1700°F and 1800°F calcines

of the Type 1 Iceland Spar material as well as by the temperature series 2061, 2062 and 2069. Decoration of the defect state by UV-irradiation producing Fe^{+++} from Fe^{++} ought to be pursued in both the limestones and their calcines.

The sensitivity of the EPR spectra to the degree of hydration in the calcines points to a very important potential use of EPR for investigating chemical reactions in these materials. One should be able to follow the conversion of $CaCO_3$ to CaO to $CaSO_3$ to $CaSO_4$ and each species should give distinguishable EPR spectra in a mixture - even with many reactions occurring simultaneously. Since EPR spectroscopy is an instantaneous measurement ($\approx$9000 "experiments" per second) kinetic studies can be done on solid-gas and solid-liquid reactions, as well as liquid-gas reactions. The EPR investigations of the chemistry of the limestone and calcine materials with SO_2 should prove to be a fruitful area - in both dry injection and wet-scrubbing processes.

REFERENCES

1. R. H. Borgwardt, Environmental Science and Technology 4, 59 (1970).

2. R. H. Borgwardt, "Isothermal Reactivity of Selected Calcined Limestones with SO_2", Paper presented at the International Dry Limestone Injection Process Symposium, Paducah, Kentucky, June 22-26, 1970.

3. M. Ishida, S. C. Wang, C. Y. Wen, "Study of Rate of SO_2 Absorption by an Agglomerated Single Sphere of Calcium Dioxide Powder" - preprint of paper, Journal or Conference Source Unknown.

4. K. S. Murthi, D. Morrison, and R. K. Chan, Env. Sci. & Tech., 5, 776 (1971).

5. R. D. Harvey, Interim Report to the National Air Pollution Control Administration, Contract No. CPA-22-69-65, June 22, 1970.

6. R. D. Harvey, Final Report, Contract No. CPA 22-69-65, July 15, 1971.

7. D. C. Drehmel, Am. Cer. Soc. Bull., 50, 666 (1971).

8. D. C. Drehmel, "Limestone Types for Flue Gas Scrubbing", Paper presented at the Second International Lime/Limestone Wet Scrubbing Symposium, New Orleans, Louisiana, November 8-12, 1971.

9. R. H. Borgwardt, D. C. Drehmel, T. A. Kittelman, D. R. Mayfield and J. S. Bowen, "Alkaline Additives for Sulfur Dioxide Control". Air Pollution Technical Data Document 0737.

10. P. K. Ghosh, M. Samaddar, S. C. Sinha, J. S. Tiwari and A. C. Banerji, Technology 7, No. 4, 276 (1970).

11. C. Kikuchi and L. M. Matarrese, J. Chem. Phys. 33, 601 (1960).

12. S. A. Marshall and A. R. Reinberg, Phys. Rev. 132, 134 (1963).

13. A. J. Shuskus, Phys. Rev. 127, 1529 (1962).

APPENDIX A

EPR THEORY AND APPLICATION TO THE CHARACTERIZATION OF SOLID-STATE MATERIALS

GENERAL THEORY

Systems with unpaired electrons exhibit a paramagnetism which serves to identify them on the application of electron paramagnetic resonance (EPR) spectroscopy in a magnetic field. This paramagnetism is due primarily to the spin angular momentum of the unpaired electron ($S = 1/2$) which can be quantized in a magnetic field such that the projection of the spin angular momentum along the axis of quantization (along the magnetic field) is $S_z = \pm 1/2$. For an isolated electron in a magnetic field, the energy is described by the Hamiltonian

$$\mathcal{H} = \beta \underline{S} \cdot g \cdot \underline{H} \qquad (1)$$

in which β is the Bohr magneton, $\underline{S}$ is the spin angular momentum, $\underline{H}$ is the magnetic field and g is a second rank tensor. For an electron, in the absence of other perturbations, the principal values of the g tensor are equal so that $\mathcal{H} = g\beta \underline{S} \cdot \underline{H}$ and two magnetic levels are possible for the electron:

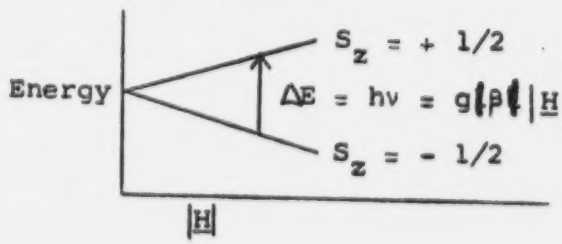

Transitions may be induced between these two levels by the application of radiofrequency energies (usually λ = 3cm at 3500 Gauss) such that

$$\Delta E = h\nu = g|\beta|\underline{H}. \qquad (2)$$

It is principally this energy absorption which gives rise to EPR spectroscopy. In practice, the microwave source is held constant and the magnetic field varied until absorption is observed, contingent on the resonant condition in equation (2).

Of course in real systems, we do not have an isolated, perturbation-free electron. The unpaired electron may be non-bonded, but in an anion vacancy in a crystal lattice; or it may be an integral part of a molecular species such as Mn^{++}, Fe^{+++}, H, NO_2, O_2^-, Ti^{+3}, Zn^{+1}, Ag^{+2}, etc. An isolated electron has no orbital angular momentum and g is a function of spin only and equal to 2.0023, but once the electron is constrained to move within a molecular or crystalline framework, a finite orbital angular momentum can result, imparting an additional paramagnetism to the electron such that g is a function of both spin and orbital angular momentum. In real systems g can vary more than 10% from the free electron value. As examination of equation (2) will show, systems with different g-values will give rise to spectra at different magnetic fields. Another distinguishing feature is the interaction of the unpaired electron with magnetic nuclei in the same species; e.g. the unpaired electron interacts with the manganese nucleus

in Mn^{++}, with the nitrogen nucleus in NO_2, with protons in H, OH, C_6H_5, and with C^{13} in natural abundance in organic compounds.

When magnetic nuclei are present the energy is best described by

$$\mathcal{H} = |\beta|\underline{S}\cdot g\cdot\underline{H} + \Sigma_i \underline{S}\cdot A_i\cdot\underline{I}_i \qquad (3)$$

in which I_i is the nuclear spin of the ith nucleus and A_i is the second rank hyperfine interaction tensor. The magnetic nuclei in effect "split" the EPR transitions in characteristic ways so that molecular structure determinations can be made. For example the nuclear spin of magnanese is 5/2 and thus each electron spin transition in Mn^{++} is split into six components, giving a six line spectrum.

For a particular paramagnetic species there are definite values for g and A_i which distinguish not only the species but also the symmetry of the species. For example it is possible to distinguish O_2^- on the surface of ZnO from O_2^- in the crystal lattice.

EPR and optical spectroscopy serve to complement one another in solid state studies. The curve under the EPR absorption curve is proportional to both the concentration and the total amount of absorbing centers, and hence EPR does

not follow Beer's Law as is the case with optical absorption. The EPR transition probability (related to the extinction coefficient) is essentially the same for the unpaired electron, regardless of the environment. Thus quantitative determination of an unidentified paramagnetic species can be easily made by comparison with a known standard. This is certainly not the case with optical investigations. Furthermore, because the magnetic environment of different species is different, the transitions for each species are distinguishable in a mixture of paramagnetic molecules which may not be the case for optical investigations in which there can be considerable overlap of absorption or reflection. The sensitivity of the method is very high, 10^{11} spins or molecules is the usual minimally detectable limit for each species. For a usual sample size of 1 cm^3, this represents 2×10^{-13} moles.

EPR is a non-destructive technique, a physical measurement not affecting the concentration of nature of the species. In optical investigations this may not be the case since (especially ultra-violet) light can actually produce additional absorbing centers. Thus the comparison of EPR and optical investigations can serve to detect the effects of optical irradiation on solid-state materials. In fact, the effects of optical irradiation on solid-state material can be determined by simultaneously observing the EPR and optically irradiating the material in the same EPR sample cell.

Reflectance spectroscopy on poly-crystalline material has been demonstrated to yield the absorption coefficient, but the studies are sometimes complicated by scattering, internal reflection, and particulate size effects. The problem of optical centers on the surface, in contradistinction to the bulk of the material, can be a complex one, one which EPR studies may clarify since the technique is so sensitive to small changes in magnetic environment and symmetry. EPR is particularly useful in resolving optical spectra in which there is a great deal of overlap of structurally similar or dissimilar species.

The species in their <u>natural</u> states to which EPR techniques may be applied are generally limited to natural paramagnetic defects in solids, a few stable free-radicals (such as NO_2), and compounds of transition metals and rare earths. However, almost any solid material can be rendered paramagnetic by several techniques: (1) γ-irradiation, which is widely utilized to decorate the defect state of solid-state material, (2) ultra-violet irradiation which can ionize species to become paramagnetic, (3) thermal ionization for low energy processes, (4) paramagnetic creation of a photo-excited paramagnetic triplet state, and (5) doping the solid with paramagnetic ions.

LINEWIDTH ANALYSIS

The highfield "line" of the six Mn^{++} transitions was chosen for linewidth analysis since it was the best resolved. Under high resolution the "line" is rather complex and a typical spectra (Type 3) is shown in Figure A1. The "line" is the first derivative of the EPR absorption of a random selection of crystallites - i.e. a powder spectra. The EPR transitions in each "line" fall into two groups, each characterized by a maximum absorption which is understandable in terms of (1) the way the transitions for the random orientations vary in intensity at different directions in the crystalline lattice and (2) the number of systems absorbing at each orientation. The theory is complex, though understood, and we will not repeat it here. Suffice it to say, the two groups are observable in Figure A1 and are designated A and B. The less perfect the lattice, the broader the EPR absorption (and first derivative) of each group will be.

Three different EPR parameters were chosen and each fitted to the reactivity and capacity data of Table 14 of Reference 6. The three parameters are designated L_1, L_2 and L_3 in Figure A1. L_1 and L_2 are, in effect, the horizontal distance (in magnetic field) between second derivative maximum and minimum points for the least-overlapped portion of each of the absorption groups. L_3 is a measure of the horizontal distance (in field) between the maximum absorption and the half-height. Both measures are used in linewidth analysis.

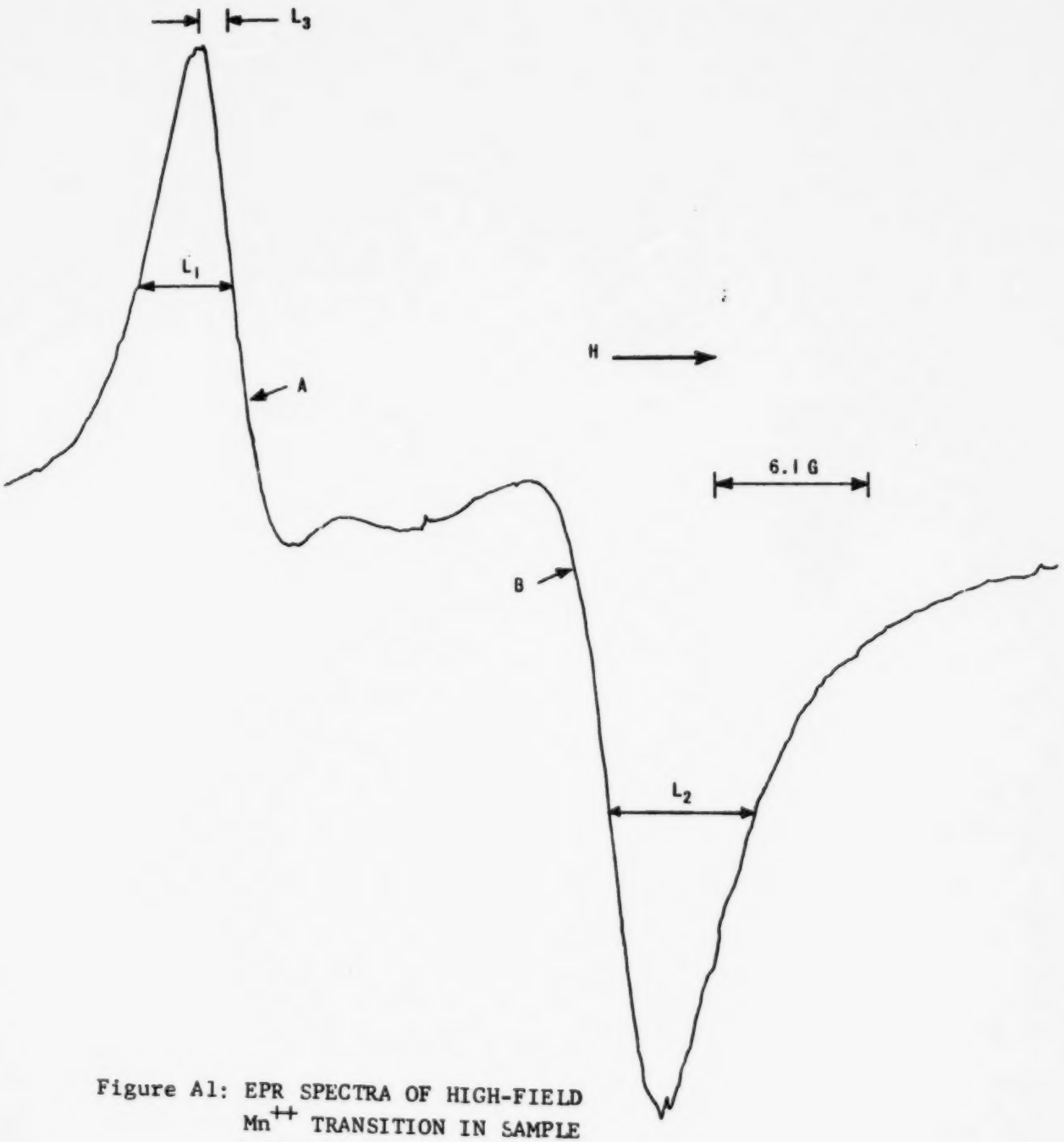

Figure A1: EPR SPECTRA OF HIGH-FIELD Mn^{++} TRANSITION IN SAMPLE TYPE 3, #2203.

APPENDIX B

EPR SPECTRA

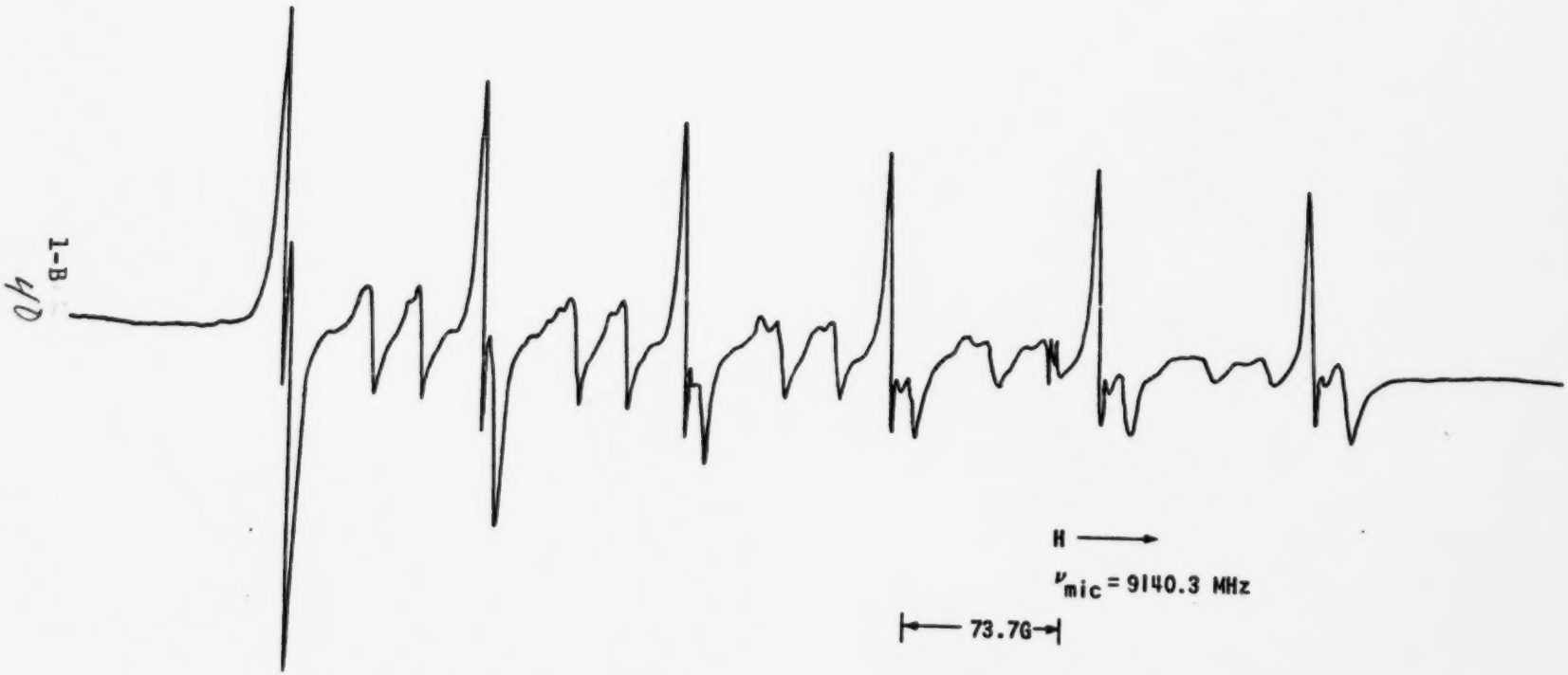

Figure B1: EPR AT ≈77°K OF SAMPLE 1336, WHITE CRUSHED MARBLE, MODULATION - 0.52G

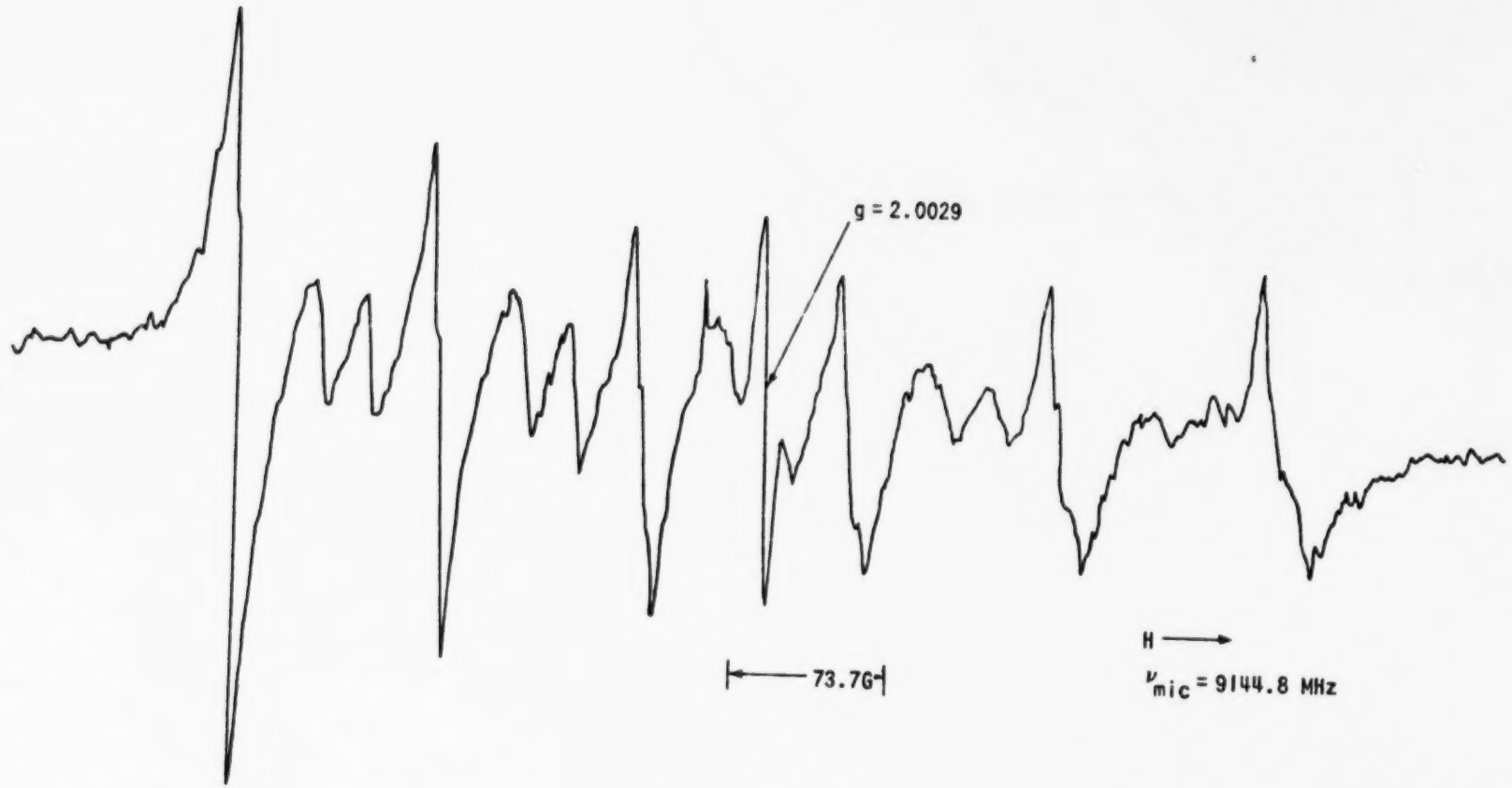

2-B
41

Figure B2: EPR AT ≈ 77°K OF SAMPLE 2129, MICHIGAN MARL, MODULATION - 0.52G

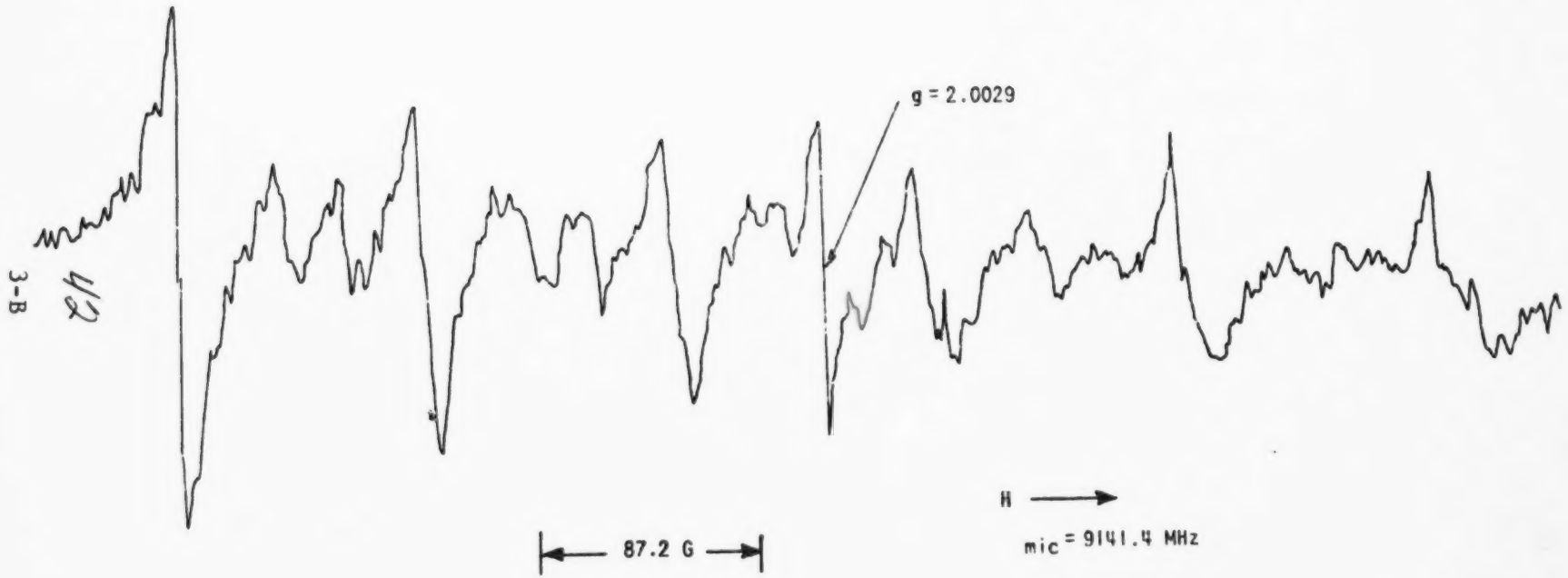

Figure B3: EPR SPECTRUM AT ≈77°K OF TYPE 11, #2129, BEFORE U.V.-IRRADIATION, MODULATION - 0.40G

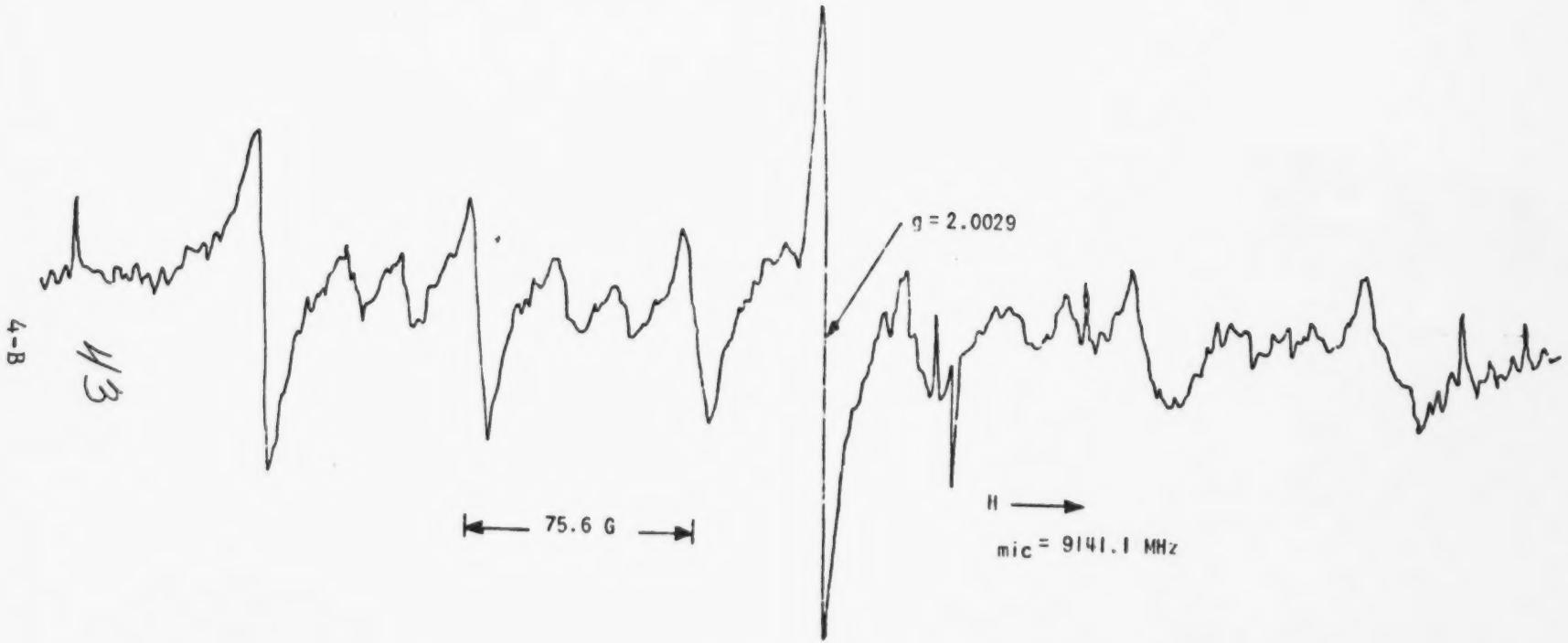

Figure B4: EPR SPECTRUM AT ≈ 77°K OF TYPE 11, #2129, AFTER 63 HRS U.V.-IRRADIATION, MODULATION - 0.39G

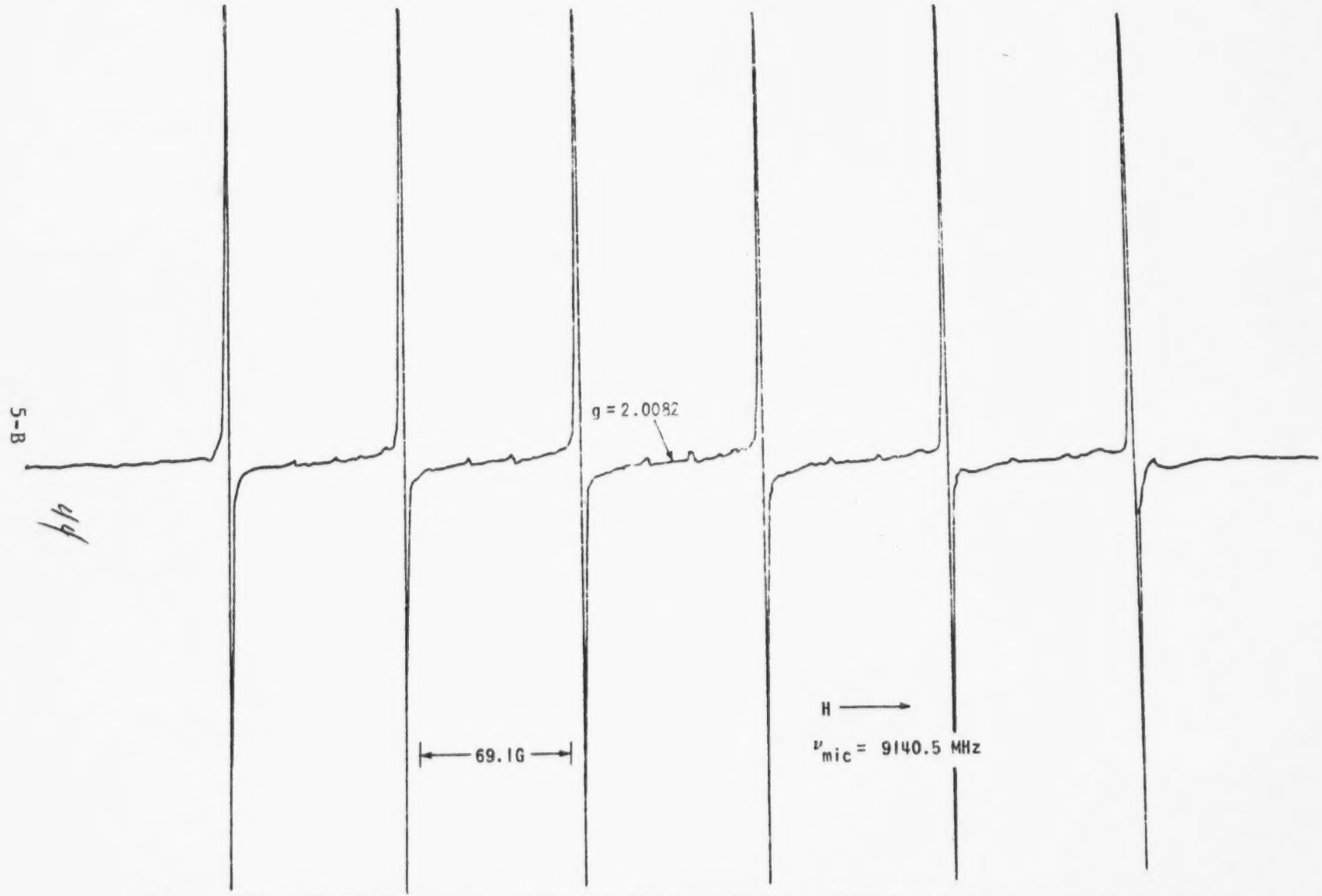

Figure B5: EPR SPECTRUM AT ≈ 77°K OF TYPE 1, #2201, 1700°F CALCINE, MODULATION - 0.40G

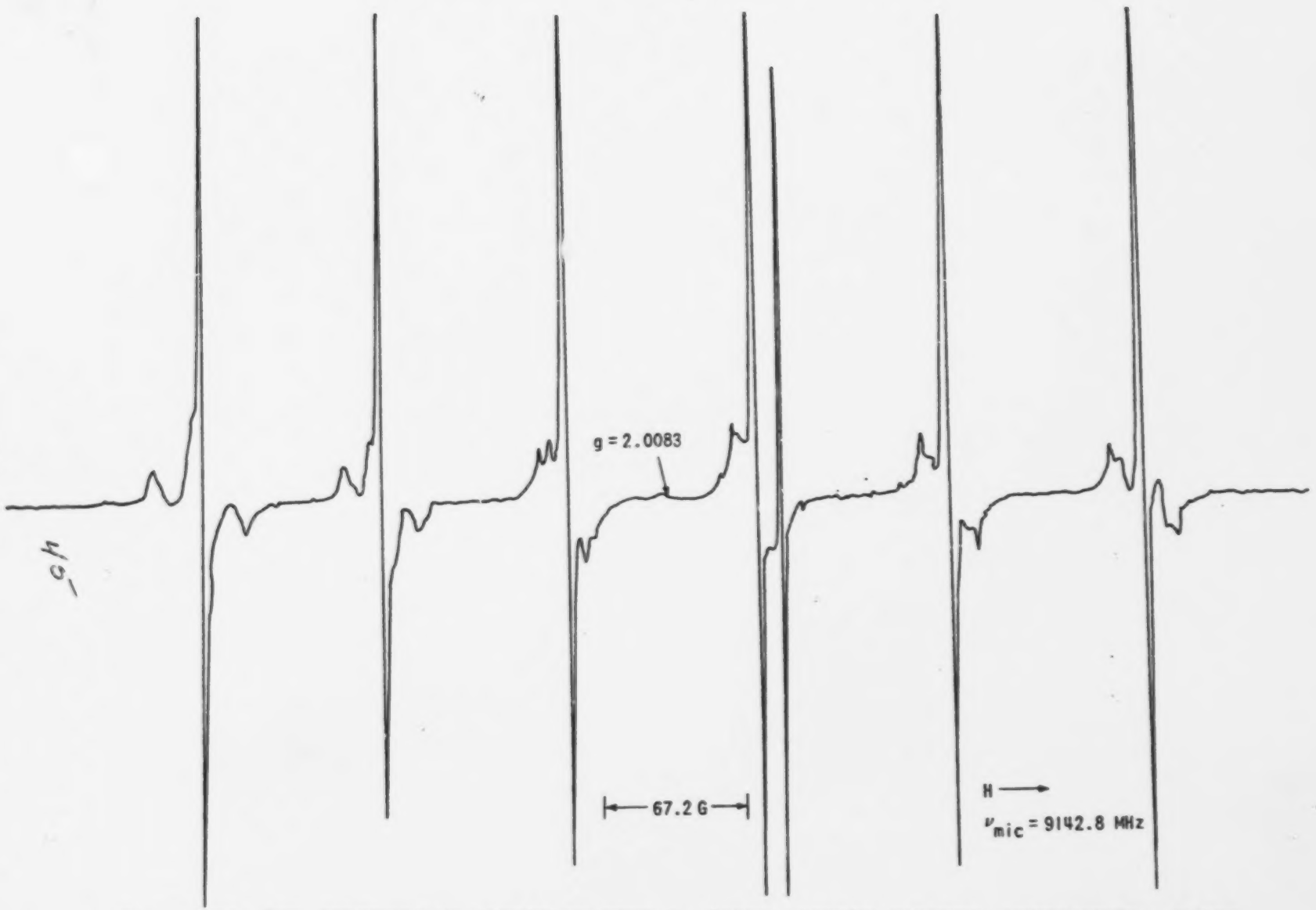

Figure B6: EPR SPECTRUM AT ≈77°K OF TYPE 1, #2201, 1800°F CALCINE, MODULATION - 0.39G

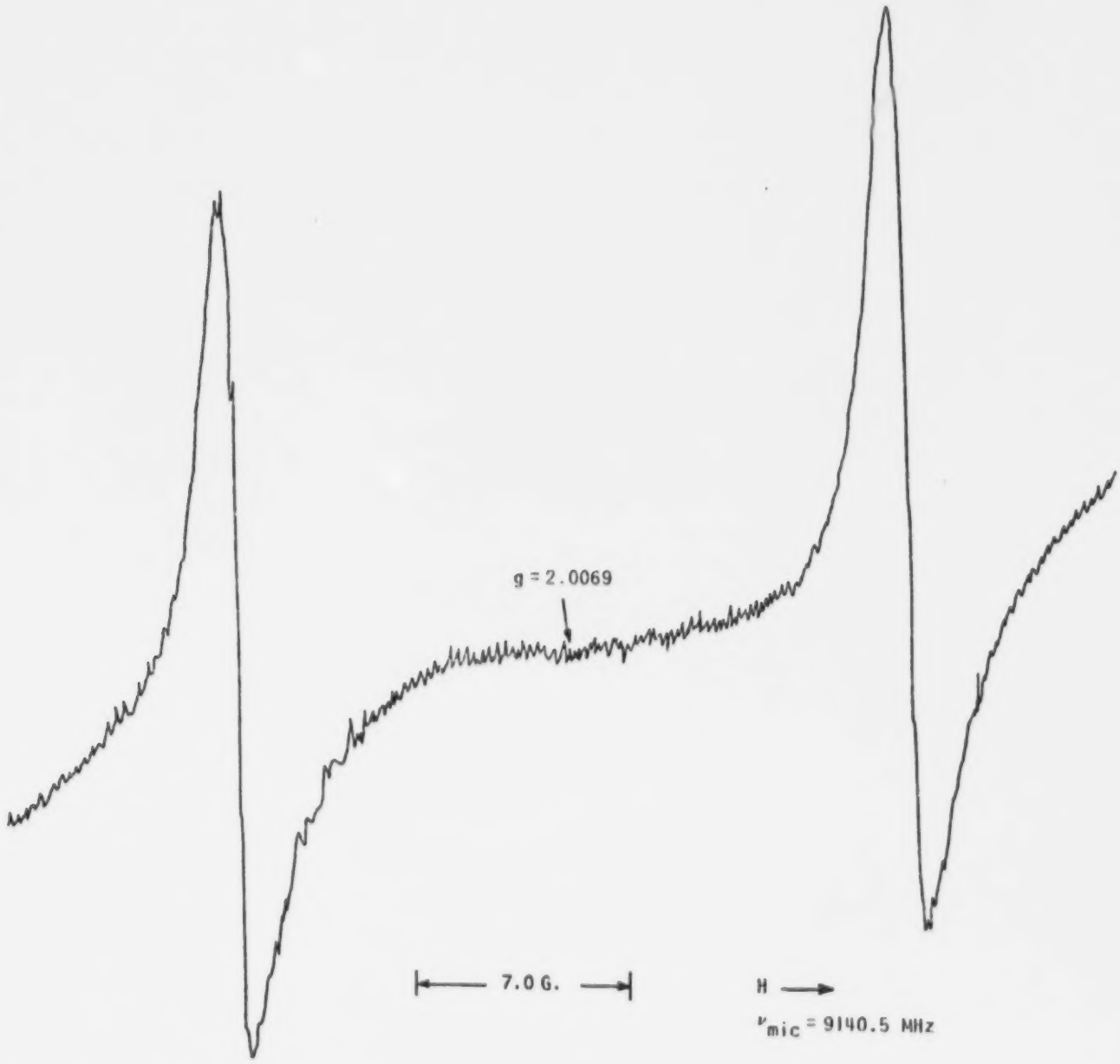

Figure B7: EPR SPECTRUM AT ≈77°K OF TYPE 1, #2201, 1700°F CALCINE, MODULATION - 1.59G.

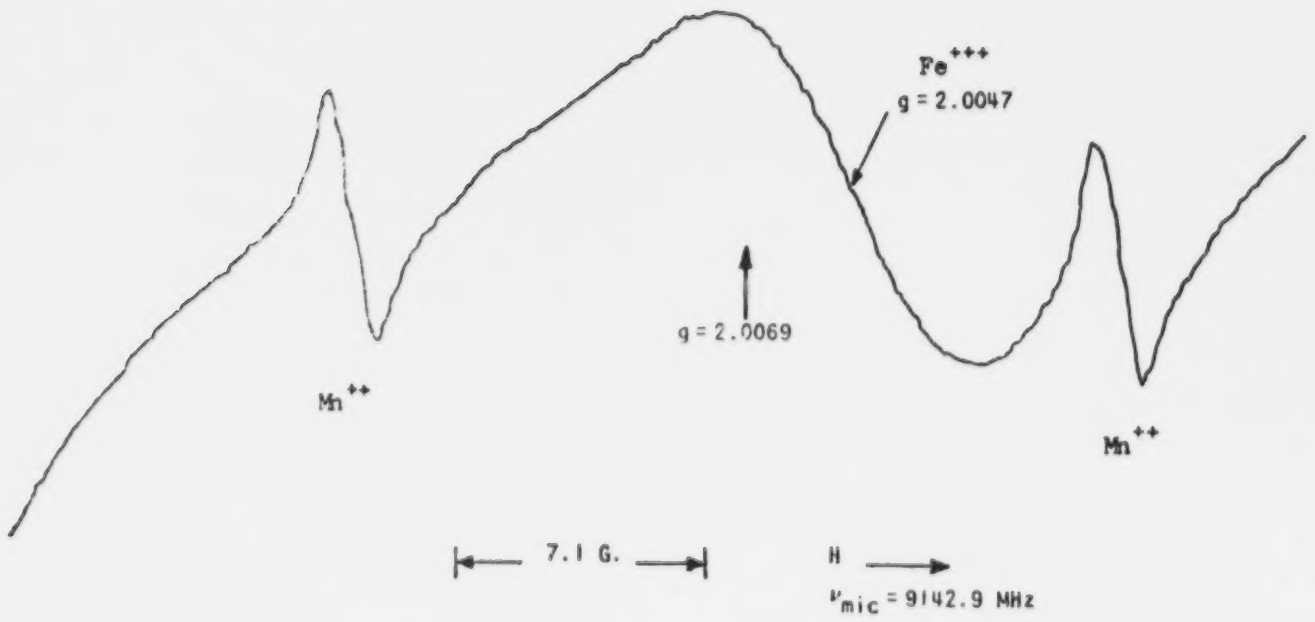

Figure B8: EPR SPECTRUM AT ≈ 77°K OF TYPE 1, #2201, 1800°F CALCINE, MODULATION - 1.60G.

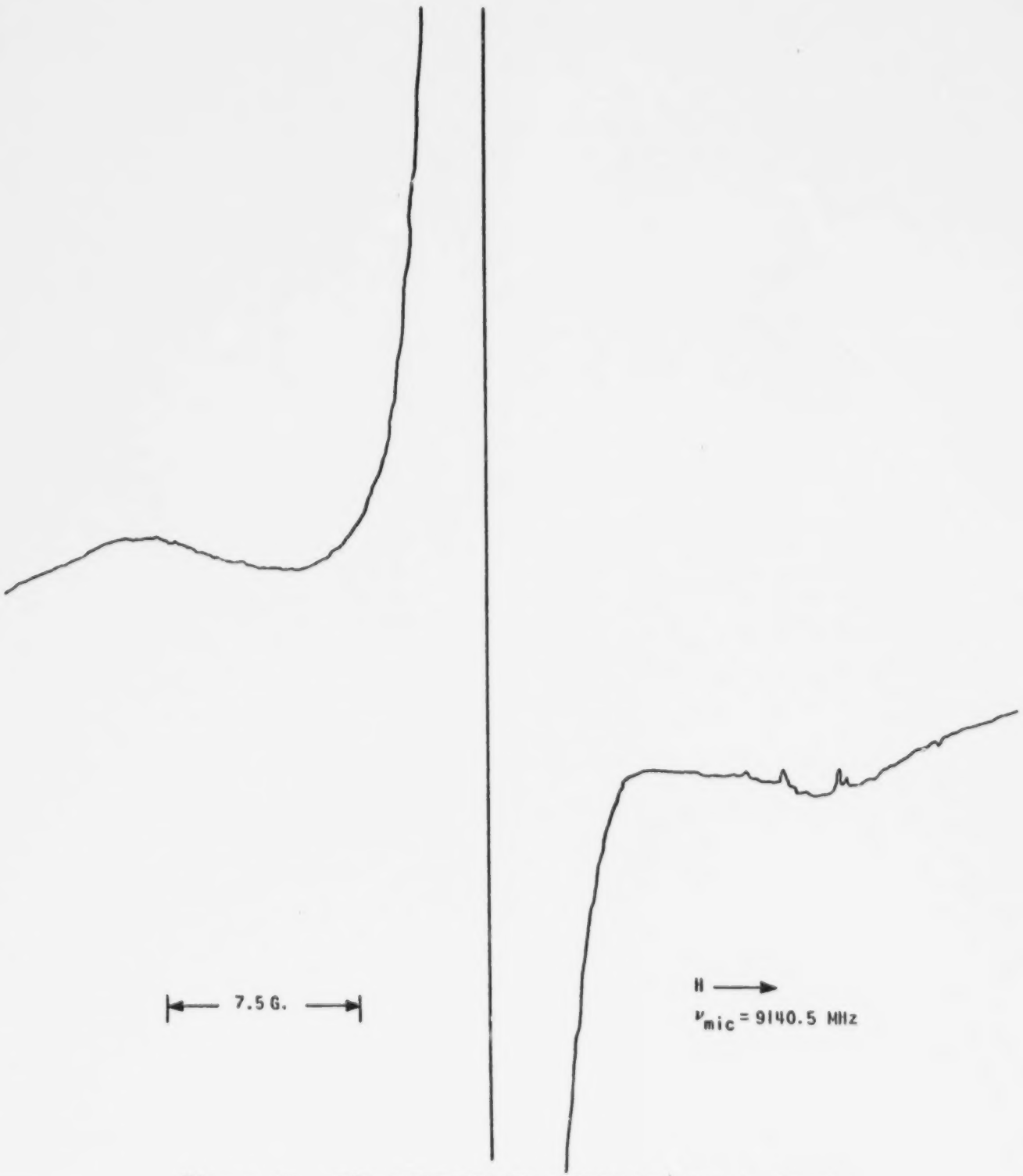

Figure B9: EPR SPECTRUM AT ≈77°K OF TYPE 1, #2201, 1700°F CALCINE, MODULATION - 0.39G.

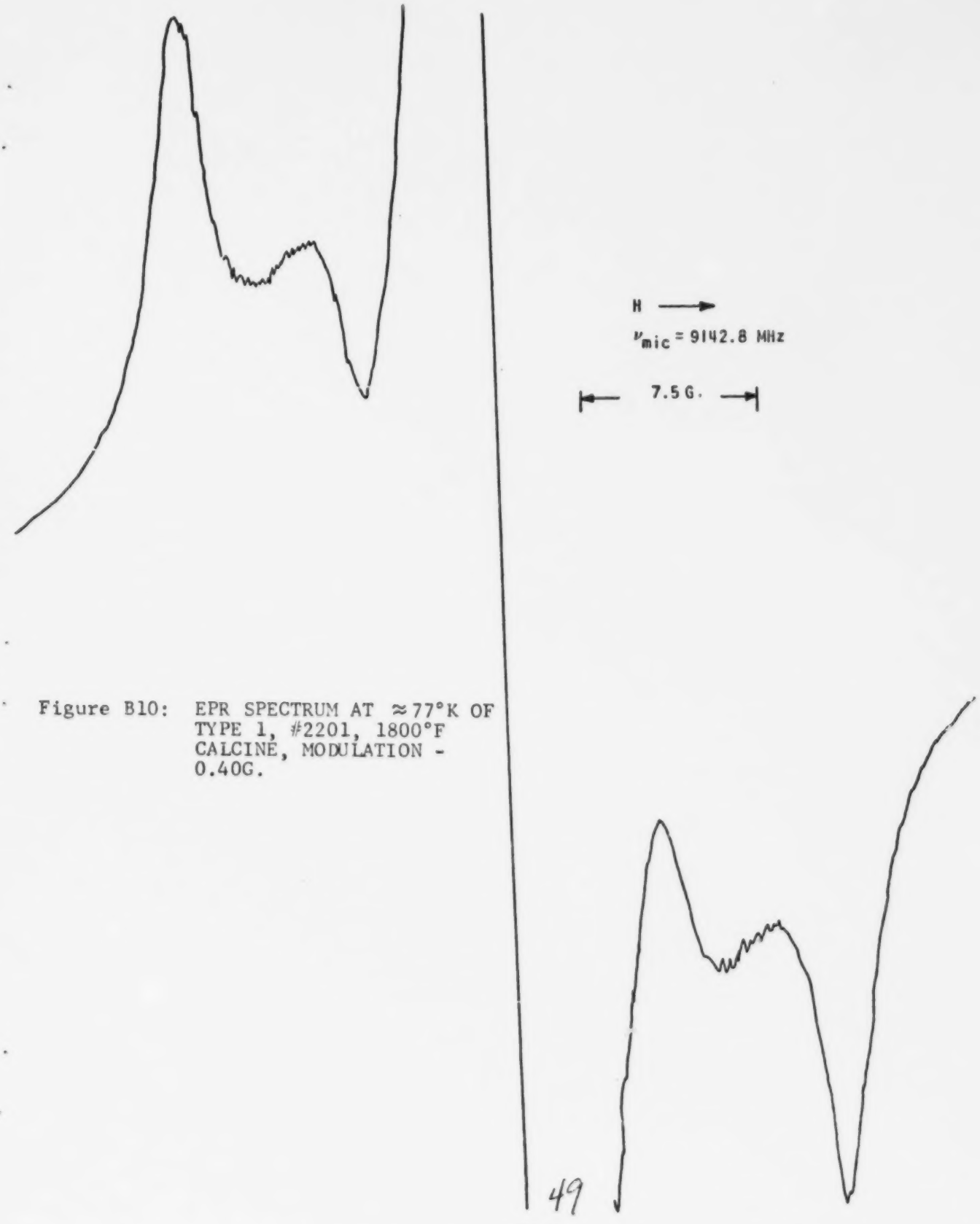

Figure B10: EPR SPECTRUM AT ≈77°K OF TYPE 1, #2201, 1800°F CALCINE, MODULATION - 0.40G.

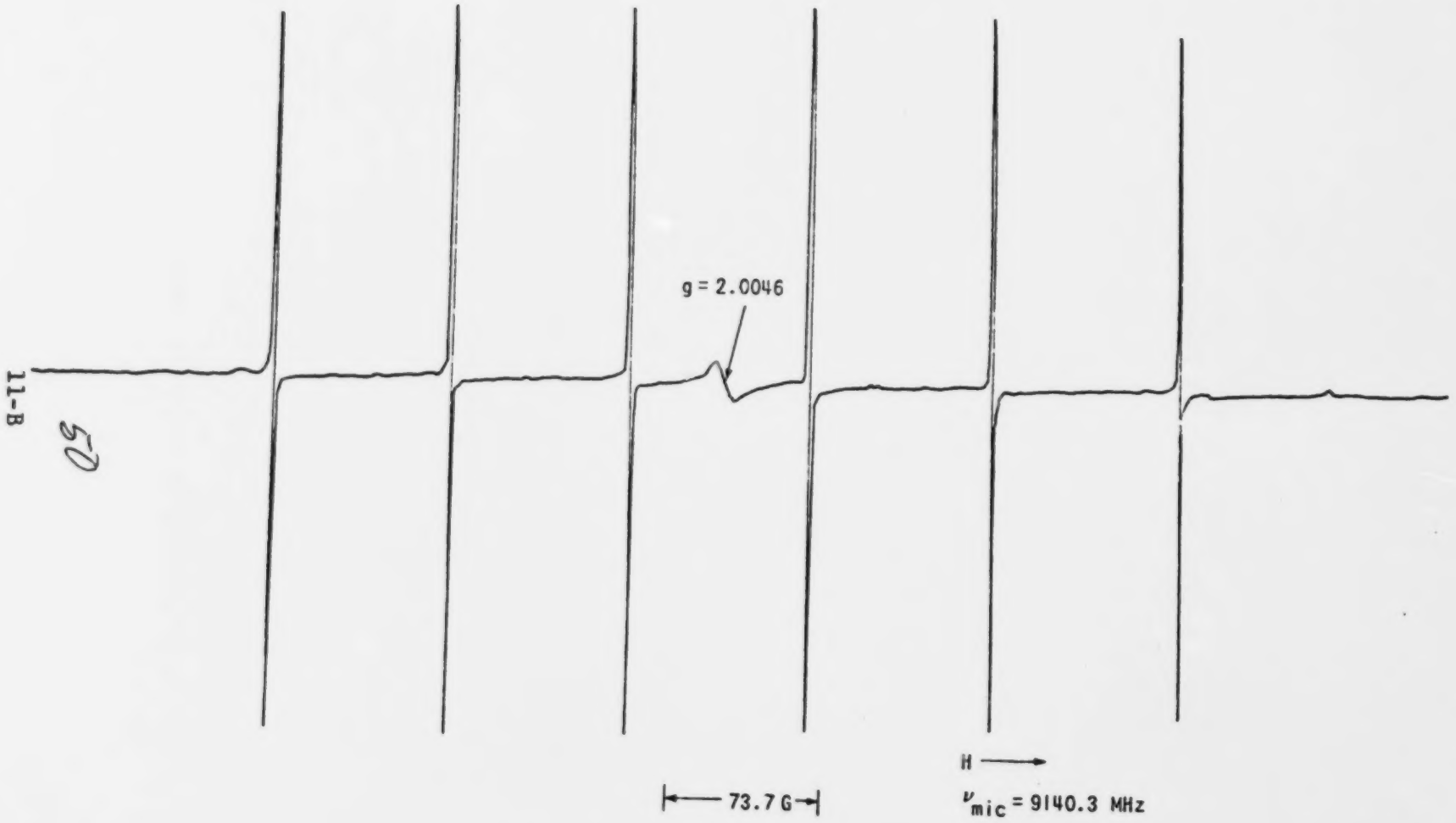

Figure B11: EPR AT ≈77°K OF SAMPLE #2061 CALCINED AT 1700°F, MODULATION - 0.52G

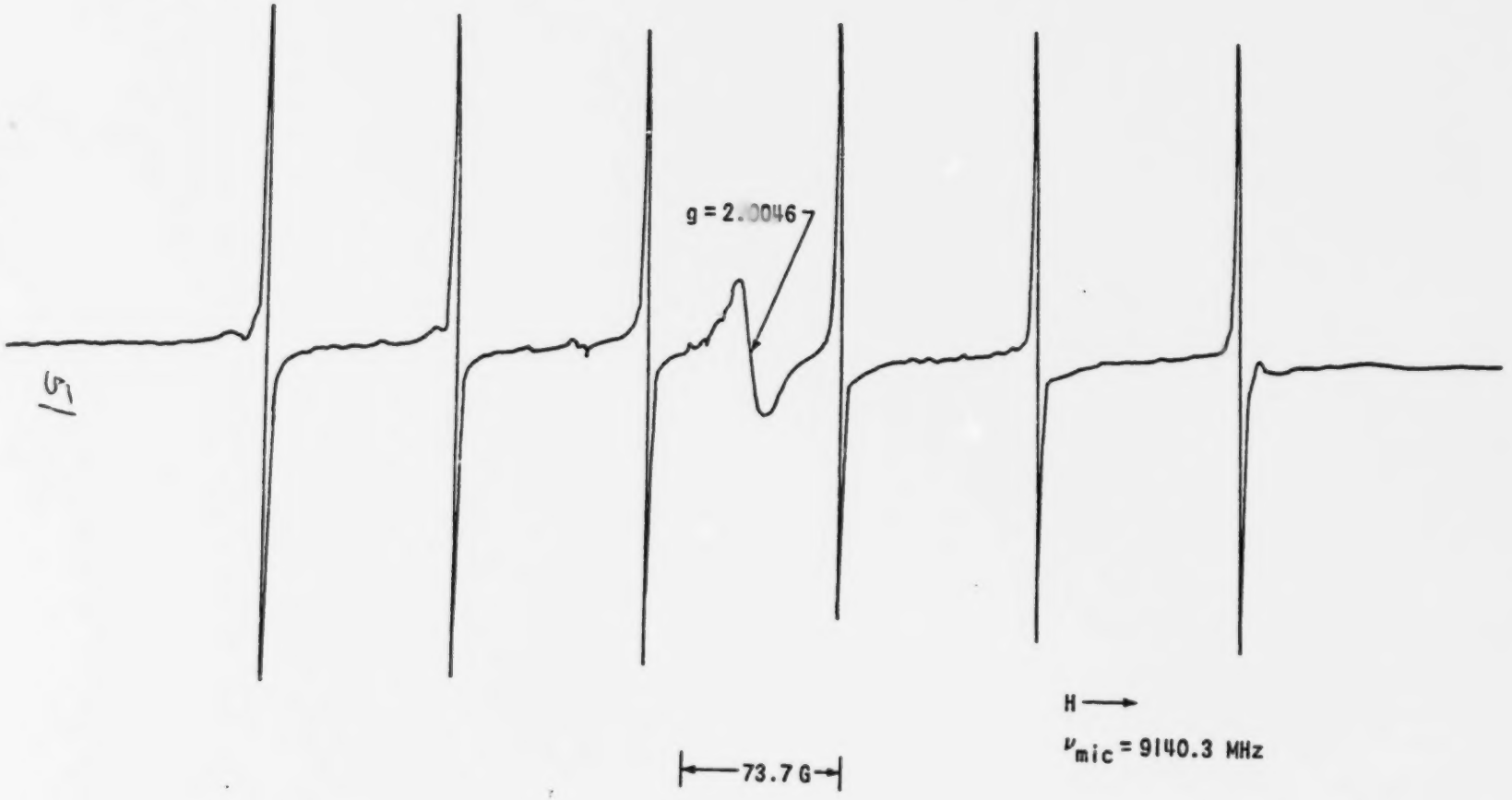

Figure B12: EPR AT ≈77°K OF SAMPLE #2061 CALCINED AT 2000°F, MODULATION - 0.52G

13-B

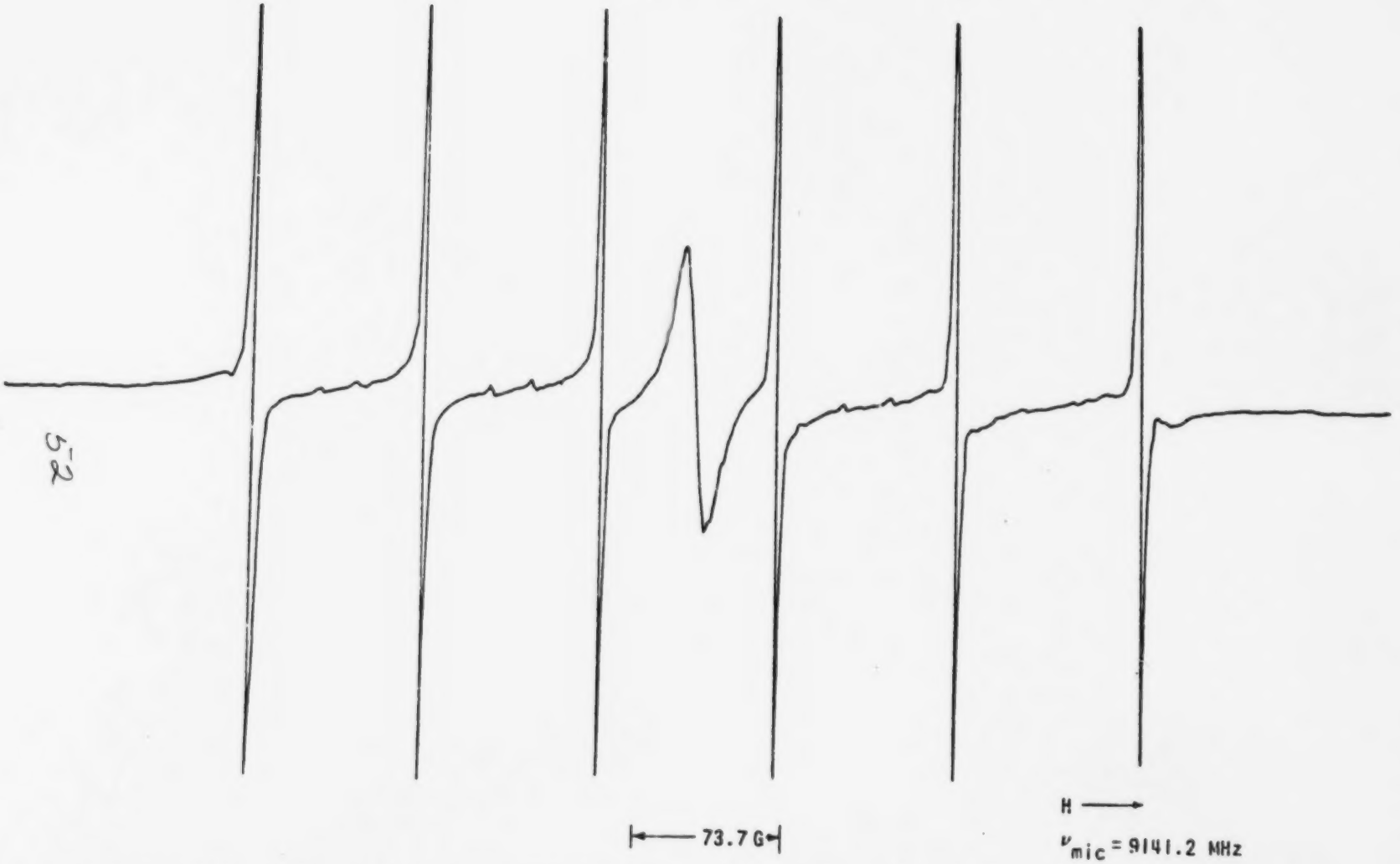

Figure B13: EPR AT ≈77°K OF SAMPLE #2061 CALCINED AT 2300°F, MODULATION - 0.52G

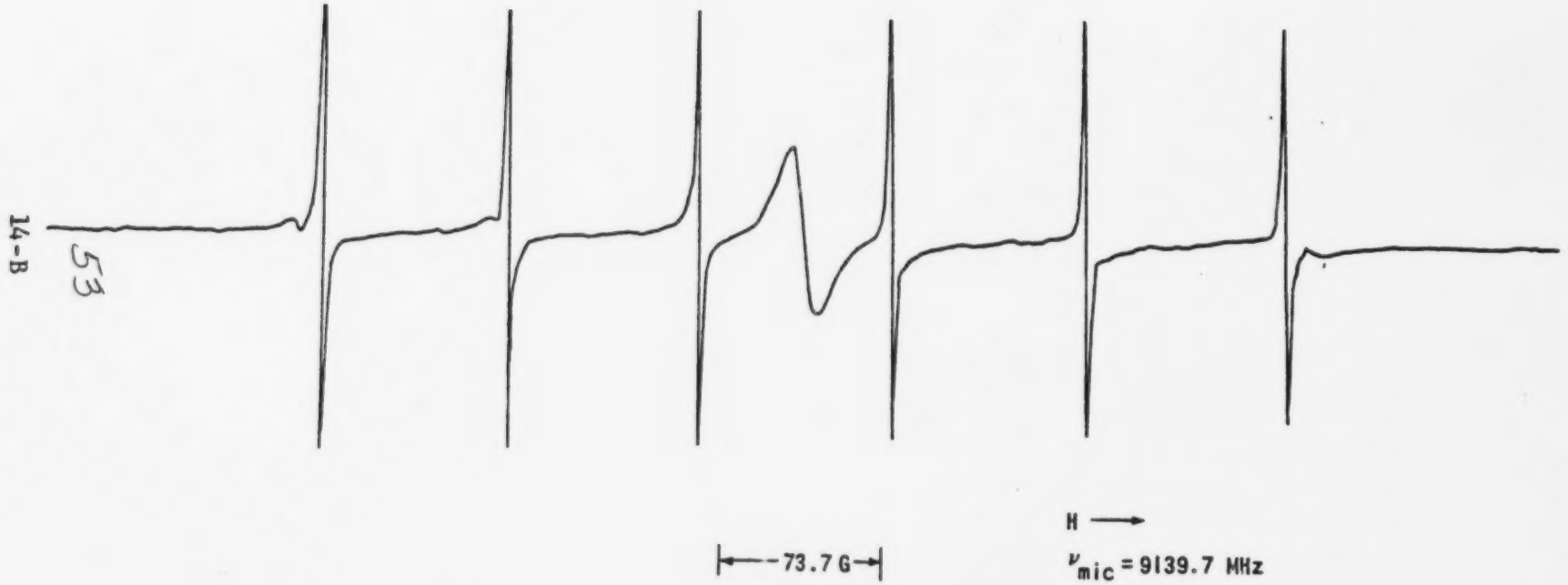

Figure B14: EPR AT ≈77°K OF SAMPLE #2061 CALCINED AT 2600°F, MODULATION - 0.52G

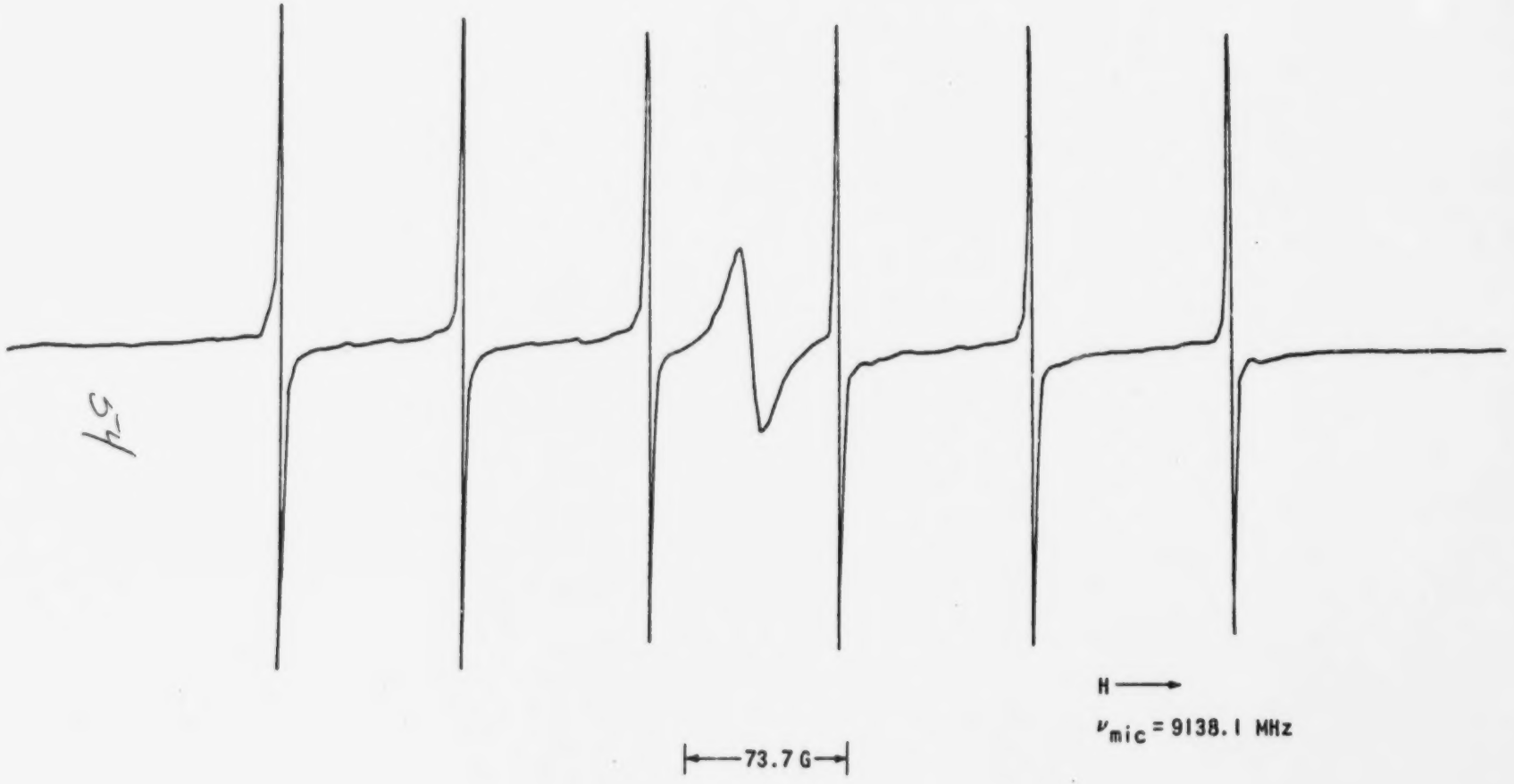

Figure B15: EPR AT ≈77°K OF SAMPLE #2061 CALCINED AT 3200°F, MODULATION - 0.52G

Figure B16: EPR SPECTRUM AT ≈ 77°K OF 1700°F #2061 CALCINED, AFTER 1 ML, 60 MIN SLAKING TEST, MODULATION - 0.45G

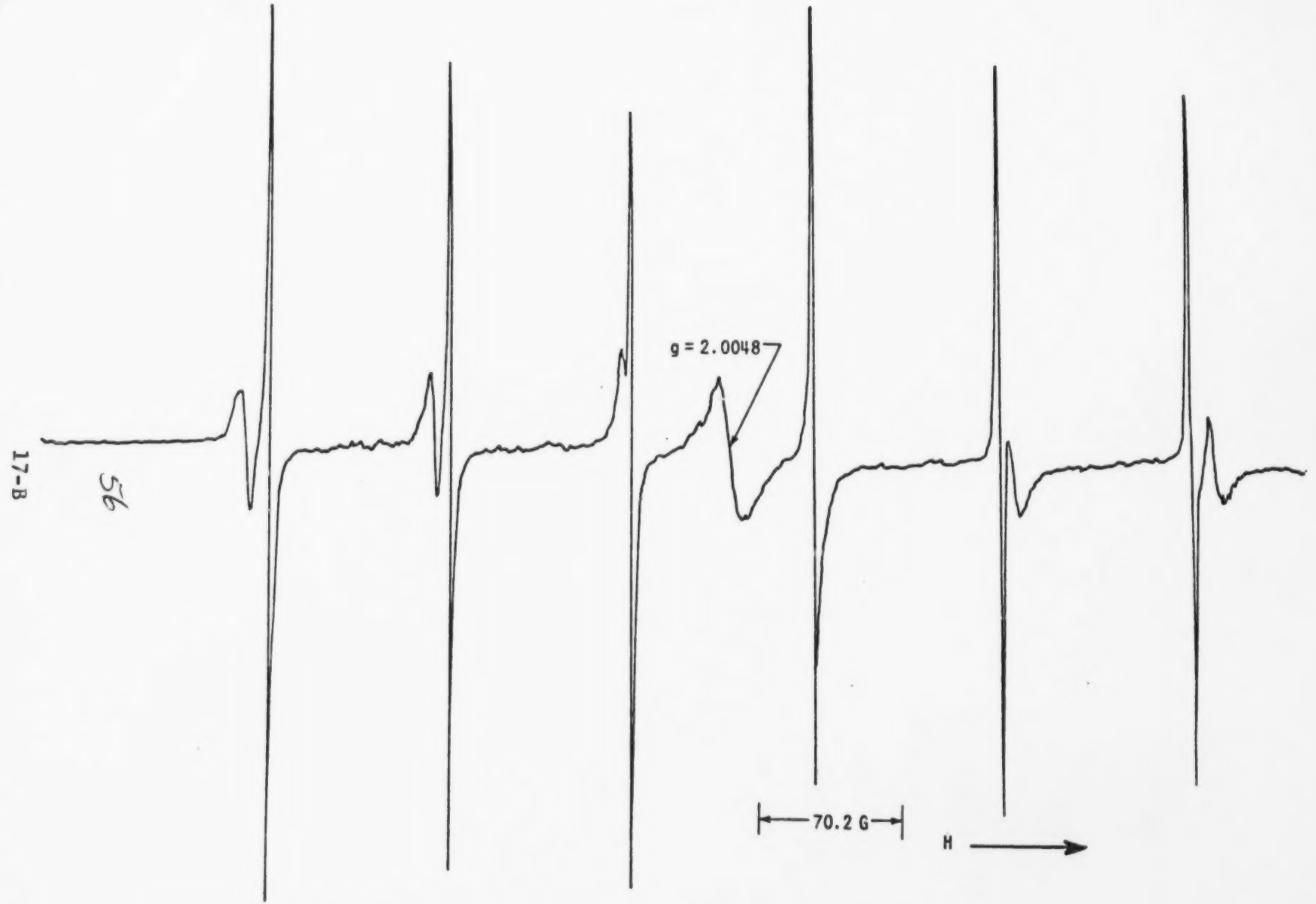

Figure B17: EPR SPECTRUM AT ≈77°K OF 2000°F 2061 CALCINE, AFTER 1 ML, 60 MIN SLAKING TEST, MODULATION - 0.45G

18-B 57

Figure B18: EPR SPECTRUM AT ≈77°K OF 2600°F 2061 CALCINE, AFTER 1 ML, 60 MIN SLAKING TEST, MODULATION - 0.45G

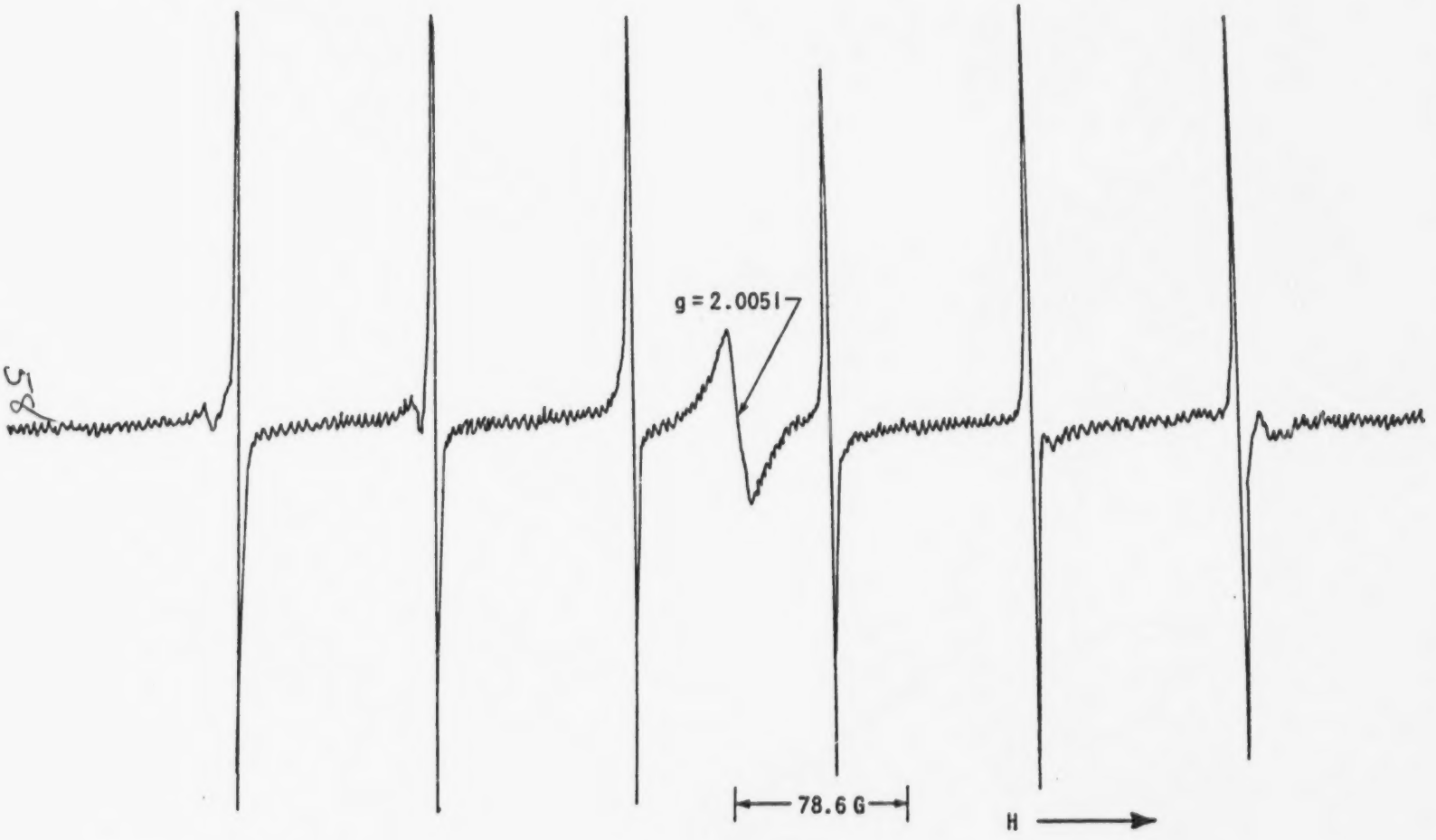

Figure B19: EPR SPECTRUM AT ≈77°K OF 3200°F 2061 CALCINE, AFTER 1 ML, 60 MIN SLAKING TEST, MODULATION - 0.45G

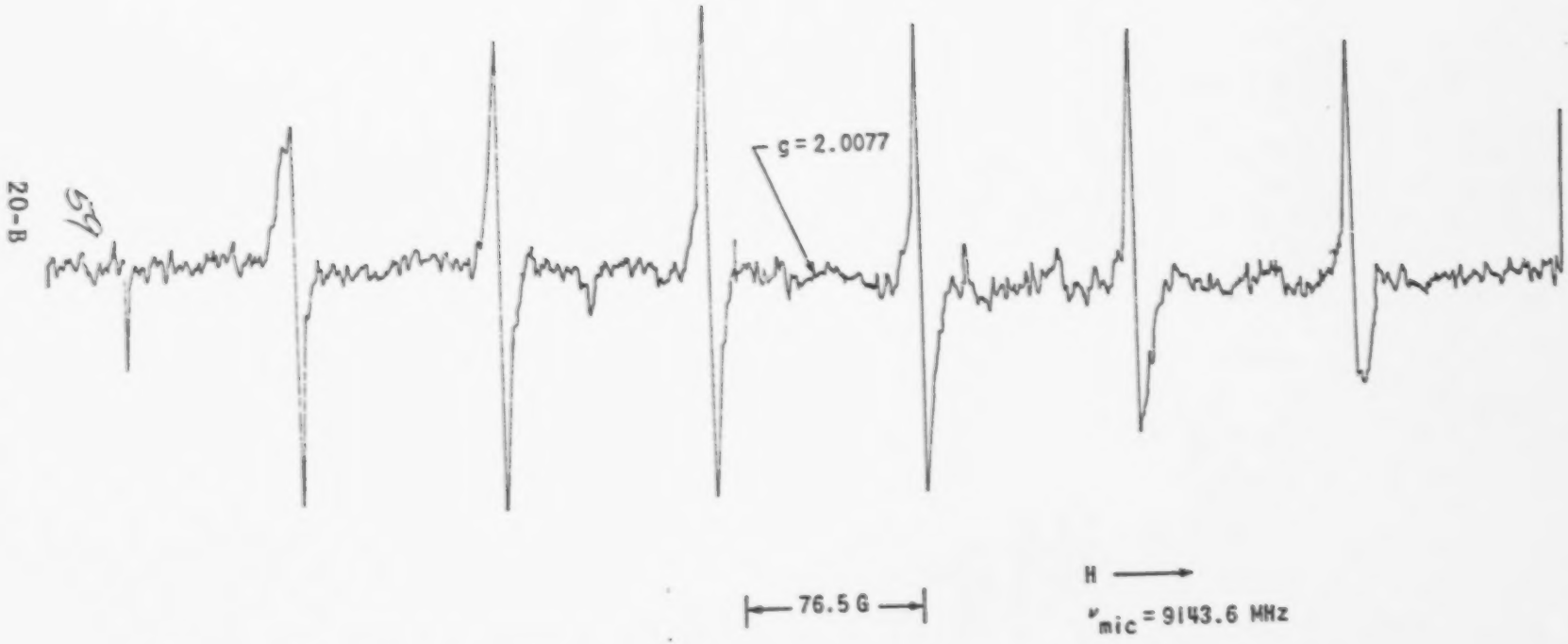

Figure B20: EPR AT ≈77°K OF 1700°F 2061 CALCINE AFTER 5 ML, 120 MIN SLAKING TEST, MODULATION - 0.40G

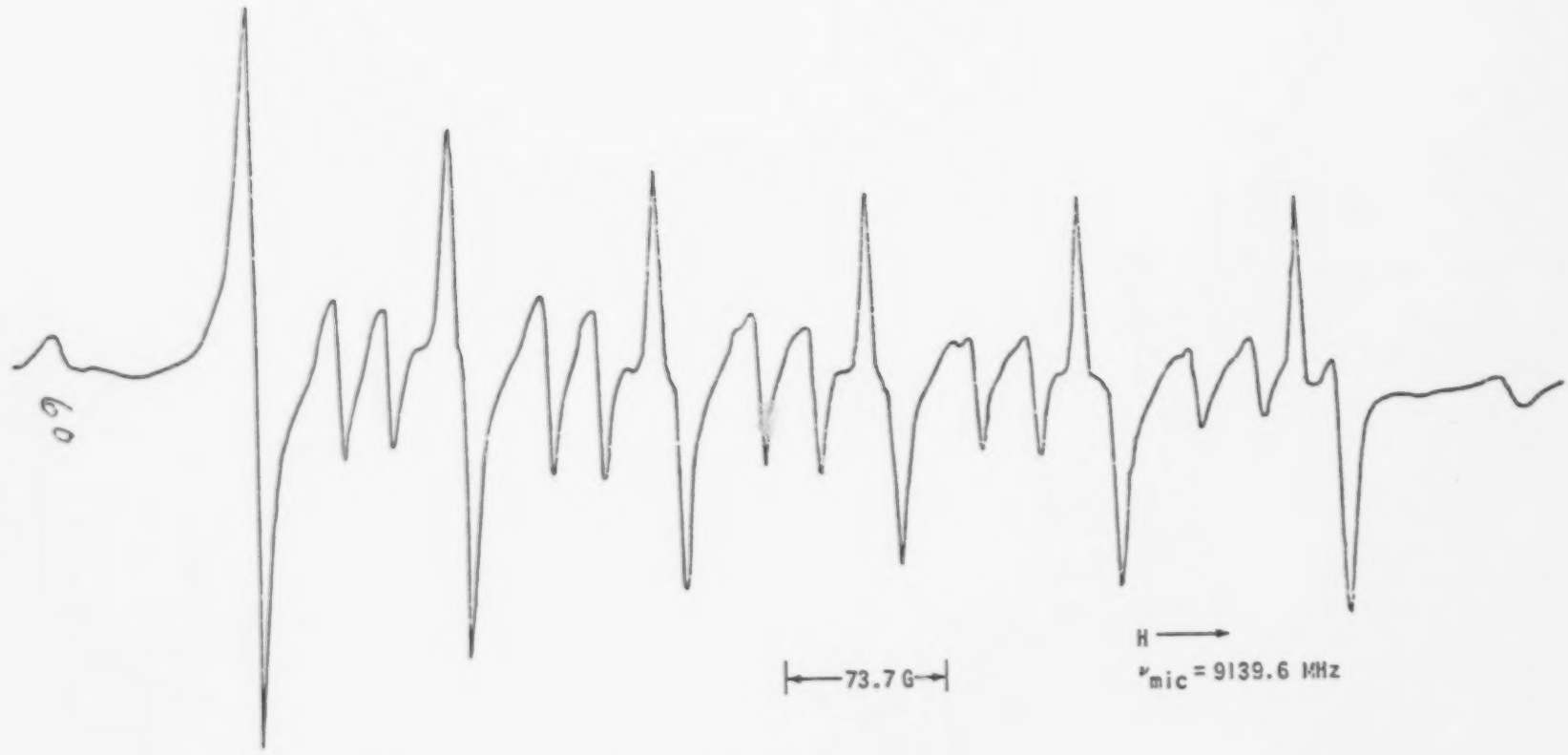

Figure B-21 EPR AT≈77°K OF SAMPLE 2203, LIMESTONE (COARSE), MODULATION - 0.52G

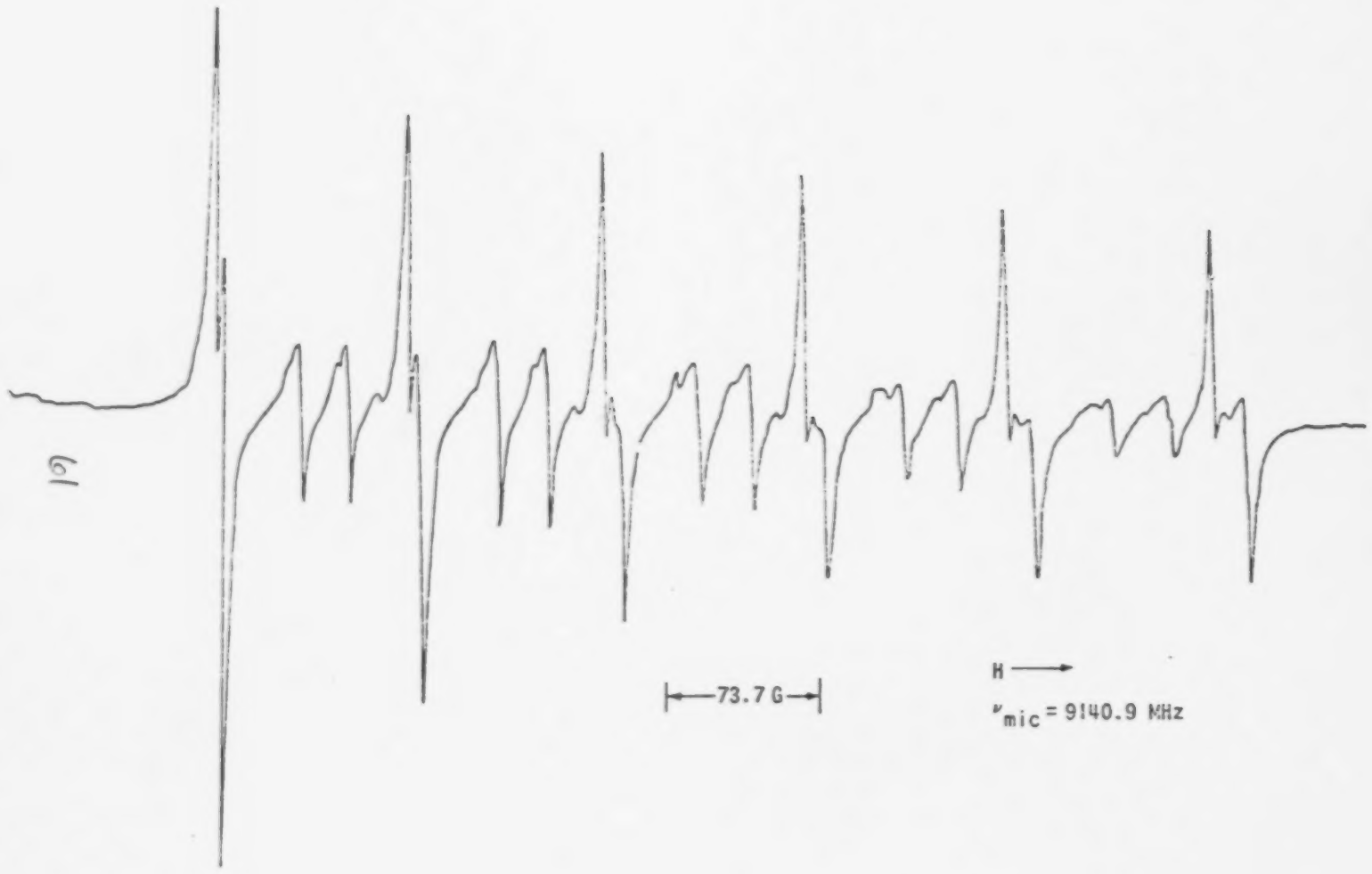

Figure B-22 EPR AT ≈77°K OF SAMPLE 2077, AUSTIN CHALK, MODULATION - 0.52G

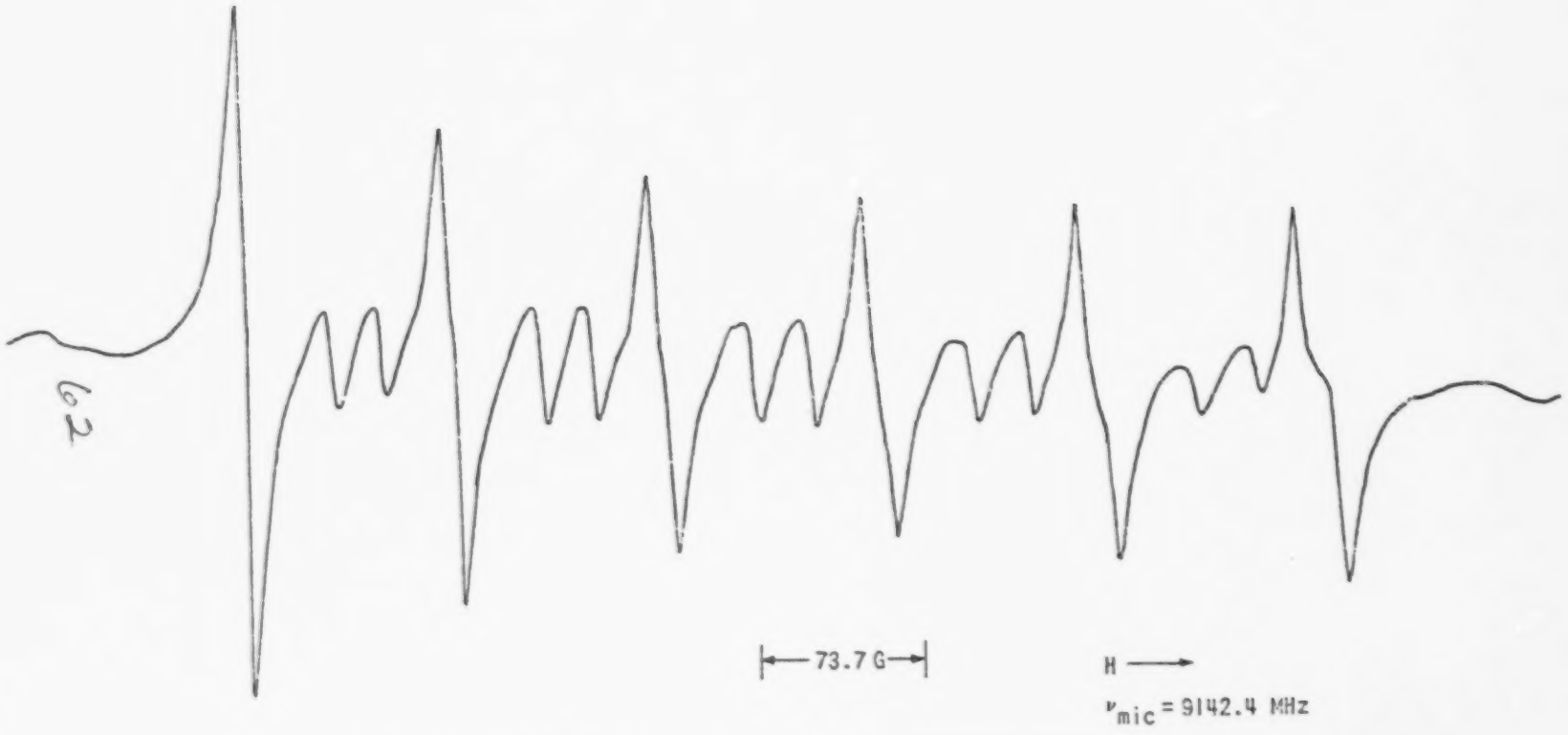

Figure B-23 EPR AT ≈77°K OF SAMPLE 2081, KANSAS CHALK, MODULATION - 0.52G

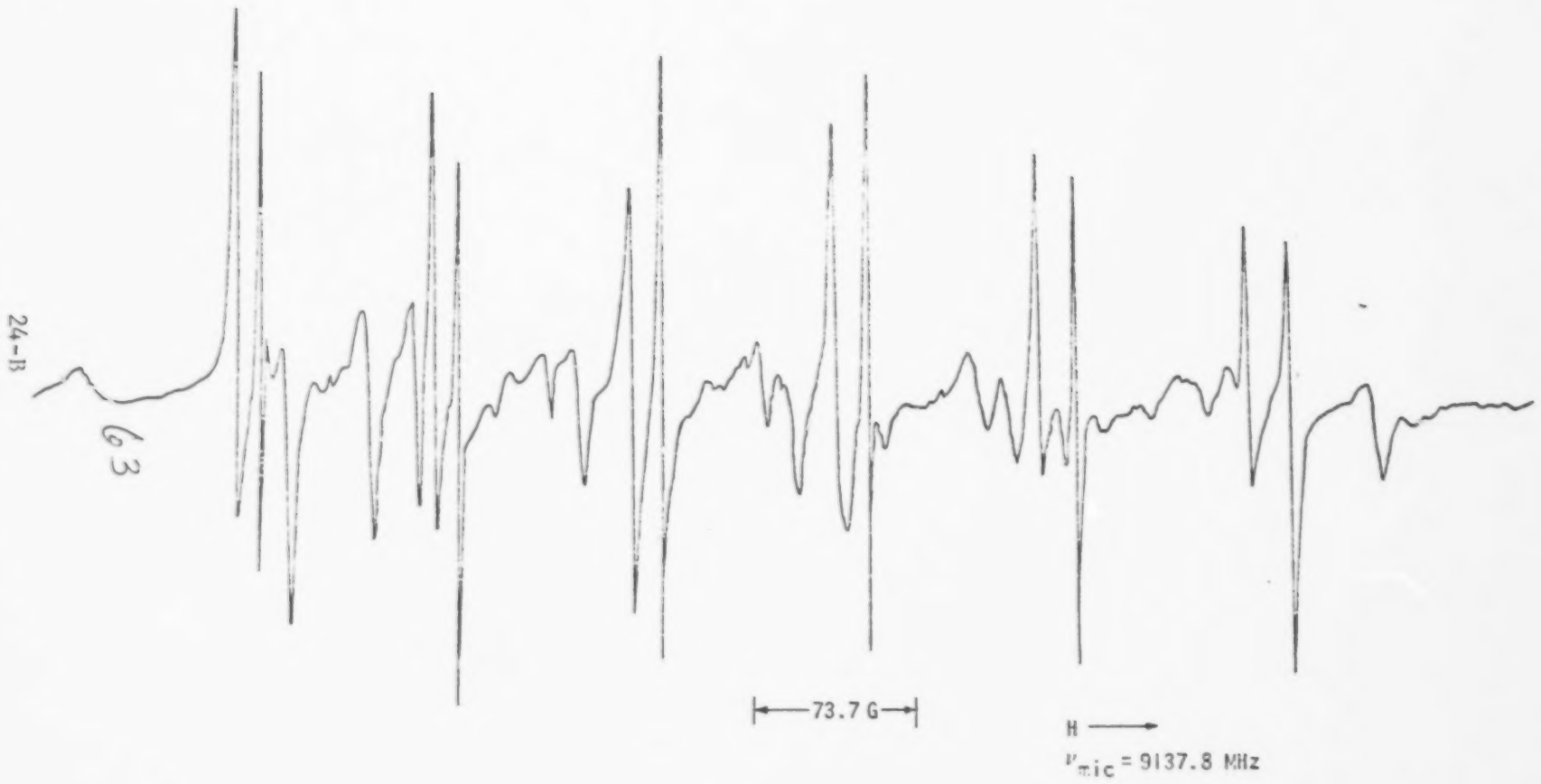

Figure B-24 EPR AT ≈ 77°K OF SAMPLE 2206, DOLOMITE, MODULATION - 0.52G

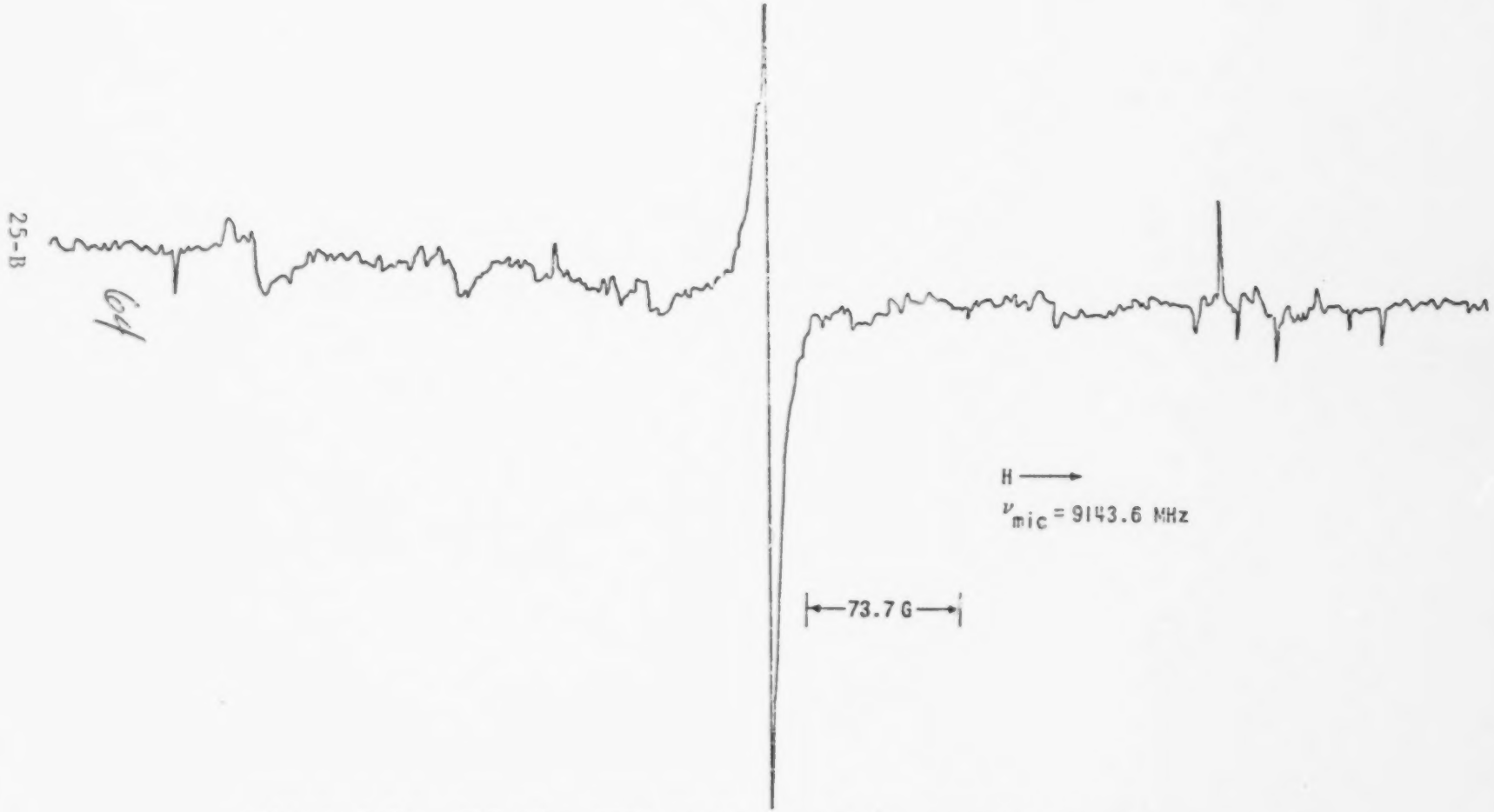

Figure B-25 EPR AT ≃ 77°K OF SAMPLE 2208, ARAGONITE, MODULATION - 0.52G

APPENDIX C

SLAKING TEST DATA

TABLE C-I

SERIES 2061 (170/200) SLAKING TEST
(Percent Weight Gain For A 1 Gram Sample)

Calcination Temperature	% Wt. loss on heating at 650°C	Soaking Volume 1ml			Soaking Volume 5ml		
		30Min	60Min	120Min	30Min	60Min	120Min
1700°F	6.5%	30.4	28.5	30.1	32.8	32.8	32.4
2000°F	3.5	-	-	24.2	-	-	-
2300°F	2.0	-	-	-	-	-	-
2600°F	5.1	-	21.5	-	-	-	-
3200°F	1.4	9.9	11.4	13.6	14.2	15.9	22.8

TABLE C-II

SERIES 2062 (-170 SIZING) SLAKING TEST
(Percent Weight Gain For A 1 Gram Sample)

Calcination Temperature	% Wt. loss on heating at 650°C	Soaking Volume 1ml	
		60Min	120Min
1700°F	3.4%	28.1	28.7
2000°F	8.3	27.0	28.2
2300°F	3.9	22.6	-
2600°F	3.4	21.4	-
3200°F	1.6	12.6	14.7

TABLE C-III

SERIES 2069 (-170 SIZING) SLAKING TEST
(Percent Weight Gain For A 1 Gram Sample)

Calcination Temperature	% Wt. loss on heating at 650°C	Soaking Volume 1ml	
		60Min	120Min
1700°F	3.3%	16.1	16.2
2000°F	3.7	10.5	-
2300°F	2.0	11.0	-
3200°F	4.0	5.3	5.3